TOPICAL REVIEW

EXAFS for liquids

Adriano Filipponi

Unità di Ricerca INFM and Dipartimento di Fisica, Università dell' Aquila, 67010 Coppito,
L'Aquila, Italy

Abstract
Extended x-ray absorption fine structure (EXAFS) spectroscopy exploits the
quantum interference resulting from the scattering of a photoelectron, generated
by the excitation of a core level, by the potential of the surrounding atoms.
From the interference pattern it is possible to determine the distance and
average distribution of the nearest neighbours from the photoabsorbing atomic
species. This spectroscopy therefore provides a unique site-selective local
structural probe in condensed matter which is ideal for investigating the average
environment of specific elements in a liquid. In the last 20 years we have
seen substantial developments in the experimental techniques which nowadays
allow scientists to perform EXAFS experiments under extreme conditions of
high pressure and temperature that were not even conceivable just a few years
ago. These techniques have been applied to the investigations of metals,
semiconductors, molecular fluids and solutions, as a function of pressure
and temperature and through phase transitions, attracting a wide scientific
community towards this spectroscopy. The complete understanding of the x-ray
absorption signal is however a challenging theoretical problem involving the
many-electron response of the system. Our current theoretical framework for
the interpretation of the EXAFS spectra is based on the solution of an effective
one-electron problem. This theory is nevertheless accurate enough to be used
in a quantitative data analysis able to retrieve valuable structural information.

1. Introduction

In the hard x-ray range, photon absorption is mainly determined by core-electron excitations.
The dominant one-electron nature of these processes is demonstrated by the existence of
main absorption edges corresponding to transitions of 1s (K-edge), 2s (L_I-edge), $2p_{1/2}$ (L_{II}-
edge), and $2p_{3/2}$ (L_{III}-edge) electrons to unoccupied states. These edges have a characteristic
energy which increases regularly with the atomic number Z. For a given element and
absorption channel, the final states involved in the transition depend crucially on their final
energy $E_f = E_i + \hbar\omega$. At the channel edge, contributions from bound resonances are often
observed, whereas above the continuum threshold E_0 (usually located a few eV above the
experimental threshold) the final one-electron states belong to the continuum spectrum. In
such a case, the photoabsorption process creates a photoelectron with a well defined energy

       R23

$\hbar\omega - E_0 = \hbar^2 k^2 / 2m$ (where k is the photoelectron wavevector and m the electron mass) which escapes from the emitting atom probing its local environment. The final state continuum wavefunction of the photoelectron is influenced by the potentials of the atoms surrounding the photoabsorber resulting in a quantum interference effect visible as an oscillation of the absorption cross-section as a function of the photon energy $E = \hbar\omega$.

The first observations of this phenomenon, which is at present commonly referred to as extended x-ray absorption fine structure (EXAFS)[1], can be dated to around the year 1920 and were made at the Siegbahn laboratory in Lund (Sweden) [1]. The first comprehensive theoretical treatment of this 'fine structure' was made by Kronig [2–4] who developed theories suitable for molecules and crystalline solids. A pioneering theoretical calculation of the fine structure for the GeCl$_4$ molecule was made by Hartree *et al* [5]. The basic understanding of the EXAFS phenomenon and of its intrinsic short-range nature was already clear from these early days of modern science. However, due to the computational limitations of the time, the validity of certain approximations could not be fully appreciated. A complete review of the historical steps towards the modern formulations of the theory of the x-ray absorption fine structure (XAFS) can be found elsewhere [6].

The application of EXAFS to the liquid (or disordered) state of matter began rather early. Mention of the collection of spectra on aqueous solutions or molecular liquids can be found in several historical papers [7–9]. However, the first experiment performed with the clear motivation of comparing the XAFS of gaseous, liquid and solid phases was performed by Dryński and Smoluchowski [10] in 1939 on GeCl$_4$ (and AsCl$_3$ [11]) molecules. These authors noticed a substantial similarity among the spectra of the gaseous and liquid phases in agreement with the qualitative understanding of the liquid state of matter available at the time and supporting the dominant molecular (and short-range) origin of the EXAFS signal in these systems.

After 1940, the potential usage of EXAFS to provide information on disordered (or liquid) matter remained latent for several decades. A controversy among supporters of a long-range against a short-range interpretation of the EXAFS developed and diverted most scientific efforts to sterile activities. Some exceptions include the work performed by a Japanese group in Osaka to apply EXAFS to the investigation of the structure of amorphous systems. They measured and compared EXAFS spectra of amorphous Ni–S alloys with those of the same samples after recrystallization [12]. Later, they compared spectra of amorphous and crystalline Ge [13], initiating what was going to become a very popular practice in later years. They realized that in spite of the amorphous x-ray diffraction pattern certain systems presented an EXAFS quite similar to some of the crystalline counterparts calling for a short-range interpretation of the signal, and, at the same time, demonstrating the existence of considerable short-range order in these systems. Similar observations were made by another group on GeO$_2$ polymorphs [14]. Short-range order theories were also supported by subsequent studies of the similarities of spectra for K$_3$[Fe(CN)$_6$] in the solid state and in solution [15].

The beginning of the modern age of EXAFS is usually considered to coincide with the publication in 1971 of the celebrated paper by Sayers *et al* [16] who proposed for the first time the possibility of inversion of the EXAFS signal using a Fourier transformation algorithm. They clearly addressed the possibility of investigating non-crystalline structures with this method and applied it to c-Ge and a-Ge. Another major breakthrough in the technique in those years was certainly associated with the development of synchrotron radiation EXAFS

---

[1] In spectroscopy the term fine structure is commonly used to indicate the splitting arising from small magnetic (spin–orbit) interactions. These effects, however, have nothing to do with the present phenomenon. In spite of such a misleading character the name EXAFS has come into common usage. The acronym XAFS was introduced later to also include the near edge structure region.

facilities which made it possible to collect excellent quality spectra in a short time. Kincaid and Eisenberger [17] at Stanford measured improved spectra of Kr, Br_2 and $GeCl_4$ in the gas phase and emphasized the limitations of the available theories to account for the observed signals. These authors also initiated the modern applications of EXAFS to aqueous solutions [18]. It was realized that the element selectivity of the x-ray absorption spectroscopy (XAS) allowed one to study the environment of a solvated ion also in the case of dilute solutions and typical Cu^{2+}–O and Br^-–O distances in the first hydration shell were determined for the first time. Similar works were performed by Sandstrom and co-workers on Ni^{2+} solutions [19,20]. Other authors in Orsay investigated more concentrated solutions and identified contributions from ionic pairing in the signal [21,22].

The first measurements of the EXAFS for a metallic liquid were made in these years by Petersen and Kunz in Hamburg [23, 24] in the soft x-ray range on Na, Al ($L_{II,III}$-edges) and Li (K-edge). These authors used a partial photoelectric yield method to measure a signal proportional to the absorption coefficient and performed the measurements under ultra-high vacuum conditions. The main motivation of these experiments was to elucidate the origin of the threshold features in terms of structural versus many-body effects predicted at the time. Crozier and co-workers performed pioneering x-ray absorption experiments on the liquid semiconductor As_2Se_3 [25] and on solid and liquid Zn [26]. In this latter paper the importance of accounting for an asymmetric atomic distribution in the data analysis was emphasized.

Although not strictly related to the liquid state, mention should also be made of the beautiful investigations performed in these years by Boyce, Hayes and co-workers [27–30] on the structure and ionic conduction mechanism in AgI and other superionic conductors. These authors tackled a rather complicated structural problem and demonstrated the power of the EXAFS technique to provide a unique insight. They developed a successful excluded volume model to describe the disordered cation distribution [28, 31] and addressed the possibility of gaining insight into the short-range shape of the interaction potential in condensed matter [29].

The status of EXAFS spectroscopy at the beginning of the 1980s is illustrated by several reviews [32–34] and books [35]. The EXAFS signal $\chi(k) = (\mu(E) - \mu_0(E))/\mu_{edge}(E)$, defined as the fractional oscillation of the absorption coefficient $\mu(E)$ with respect to the atomic background $\mu_0(E)$, as a function of the photoelectron wavevector $k = \sqrt{2m(E - E_0)}/\hbar$ (calculated with respect to a guessed continuum threshold E_0), and normalized to the atomic cross-section of the edge under consideration $\mu_{edge}(E)$, was written as the sum of single-scattering contributions from each shell j containing N_j equivalent neighbours with a Gaussian distribution of variance σ_j^2 around the average distance R_j. For K-edges and after a polarization average:

$$\chi(k) = \sum_j \frac{N_j}{k\,R_j^2}\,e^{-2R_j/\lambda_j(k)}\,|f_j(k,\pi)|\,\sin\left(2kR_j + 2\delta_1'(k) + \phi_j(k)\right)\,e^{-2\sigma_j^2 k^2} \tag{1}$$

where $|f_j(k,\pi)|$ and $\phi_j(k)$ are the backscattering amplitude and phase function of the neighbours j, $\delta_1'(k)$ is the $\ell = 1$ phaseshift for the photoabsorber atom, and $\lambda_j(k)$ is a phenomenological mean-free-path term accounting for inelastic losses. In spite of the numerous approximations contained in this approach and the total inadequacy of a Gaussian shell model for describing atomic distributions in liquids, this expression is, quite surprisingly, still widely used today to interpret spectra of liquid phase samples. The more general expression where the sum over the shells and the so called EXAFS Debye–Waller factor $\exp(-2\sigma_j^2 k^2)$ are substituted by a proper integration over a pair distribution function $g(r)$ was available [33] and was exploited quite early [26], but it has not become as popular as it should have been. A valuable reference monograph on the effect of disorder on EXAFS can be found elsewhere [36].

The recent history of EXAFS and of its application to investigate the liquid state of

matter is unfortunately rather inhomogeneous from the point of view of the scientific quality. The popularity of the technique and the intrinsic simplicity of equation (1) have attracted a wide scientific community of physicists, chemists, biologists and earth scientists, with the perspective of finding simple solutions to several applied structural problems. As a result of this, a considerable development of theoretical as well as experimental techniques has occurred in the last 20 years. At the same time, however, the unavoidable conduction of scientific work without full knowledge of approximations and limitations in our understanding of such a complicated physical phenomenon, has led sometimes to ambiguous results and mistakes.

It is the purpose of this review to illustrate the major advances in EXAFS spectroscopy as applied to the liquid state of matter that have occurred over the last 20 years. An area of extraordinary development has been that of the experimental techniques able to generate non-standard and extreme sample environment conditions. The major achievements in this field are reviewed in the next section 2, separate from the discussion of the actual scientific applications which is reported in section 5. The theoretical framework behind the modern data analysis is illustrated in section 3, while specific issues for the data analysis for liquids are discussed in section 4. Several considerations will apply also to disordered systems in general, such as glasses and amorphous covalent solids. For the theoretical part, consideration is taken of the recent publication of a review article on the XAFS theory [37] in order to avoid duplication, and emphasis is given to the issues more strictly related to the treatment of disordered matter.

2. Experimental methods

In recent years there have been enormous developments in experimental techniques. The possibility of performing physical measurements under extreme high-pressure and/or high-temperature conditions has opened novel fields of investigation and has attracted a wide scientific community towards the EXAFS spectroscopy.

This section will mainly focus on the experimental aspects of various techniques suitable for the collection of high-quality x-ray absorption spectra in the transmission detection mode. For bulk samples, this is the most effective way to measure the absorption coefficient of a substance, that (assuming an exponential decay $I_1(x) = I_0 \exp(-\mu x)$ of the beam intensity as a function of the distance x through the sample) is in practice calculated as $\alpha(E) = \ln(S_0/S_1) = \ln(I_0/I_1) + \ln(\epsilon_0/\epsilon_1)$. The S_i are the output signals from transmission detectors, such as ionization chambers, placed before and after the sample, which are proportional to the intensities of the incoming I_0 and transmitted I_1 beams through weakly energy-dependent efficiency functions ϵ_i. The second term can be eliminated by running a blank reference spectrum without sample (although this is not usually done), apart from this $\ln(\epsilon_0/\epsilon_1)$ smooth underlying background function $\alpha(E) \approx \mu(E)\,d$, where d is the sample thickness.

This expression assumes that each portion of the x-ray beam is exponentially attenuated in the same way through the sample and therefore requires the usage of homogeneous samples with a uniform thickness. Considering that the optimal thicknesses for x-rays is of the order of 10 μm it can be understood that homogeneity is by far the most challenging experimental problem for liquid samples, which often require confinement under extreme conditions of high temperature and high pressure. In the presence of a thickness distribution non-linear effects are found to reduce the contrast in the spectra [38, 39]. In the context of measurements of liquid phase samples [40], it has been shown that the experimental absorption signal can be expressed in a series expansion of the cumulant generating function $\Phi_d(t)$ of the thickness distribution $f(d)$ as:

$$\alpha(E) = -\Phi_d(-\mu(E)) \simeq \mu(E)\,\overline{d} - \tfrac{1}{2}\mu(E)^2\sigma_d^2 + O(\mu^3) \tag{2}$$

where $\bar{d}$ represents the average thickness and σ_d^2 the thickness variance.

An additional contribution to the apparent absorption of a sample $\alpha(E)$ comes from the scattered radiation. The energy variations of this contribution are usually negligible for disordered or powder crystalline samples. For single crystals, instead, Bragg reflections will occur at precise photon energies (depending on sample orientation) giving rise to a sequence of narrow apparent absorption peaks in the spectrum whose density increases considerably with energy. This occurrence largely limits the usage of single-crystal (diamond) window materials for XAS.

The confinement of a liquid sample in a shape suitable for EXAFS investigations is therefore a challenging experimental problem. This issue was clearly addressed in the pioneering investigation on liquid $GeCl_4$ [10] where a quartz cell ending with a sealed capillary was built adopting a non-ideal cylindrical sample geometry to allow for an easier and cleaner confinement. Most of the currently used techniques fall between the two classes illustrated schematically in figure 1. In the first strategy shown in figure 1(a) a typical sample mounting is shown where the liquid specimen is confined between two flat windows. This arrangement is suitable for the study of aqueous solutions with gaps of the order of 1 mm and also for pure specimens, such as molecular liquids, with typical gaps in the range 10–30 μm. The window material has to be inert in the required pressure–temperature range, stiff and sufficiently transparent to x-rays, which are often incompatible properties.
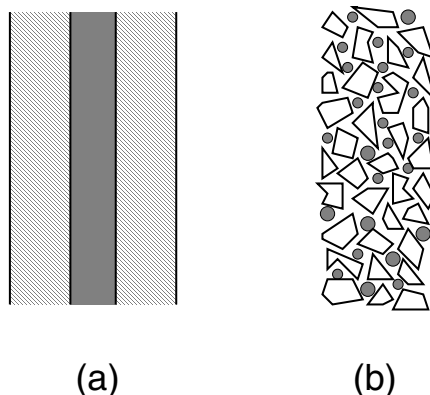

(a)   (b)

Figure 1. Schematic cross sections of typical sample geometries for XAS experiments on liquid specimens. In case (a) a thin layer of liquid is confined in the gap between two flat windows. In case (b) the sample is finely dispersed in an inert matrix. The example illustrates the shape of a sample obtained by mixing micrometric powders of sample and matrix specimens (light polygons) above the melting point where the former melt and transform into micrometric droplets (dark circles).

In the second strategy, illustrated in figure 1(b), the sample is subdivided into micrometric sized particles and dispersed in an inert matrix (in the form of powder, glue, wax ...). Above the melting point T_m the sample particles transform into a collection of micrometric droplets embedded in the matrix. A sufficiently uniform effective sample thickness distribution is obtained when the size of the particles is about 1/10 or less of the average required thickness. Examples of these types of sample are emulsions of low melting point metals [40] and sample/low-Z matrix powder mixtures [41] used for high-temperature measurements.

An evaluation of these two sample geometries involves three important aspects: (1) the sample stability during phase transformations, (2) the sensitivity to sample density variations, and (3) the resistance against contamination. For issue (1), in case (a), phase changes accompanied by volume expansion may generate enormous internal pressures that

will eventually break the cell. By comparison, for (b) type samples the particles have usually enough space to expand (or shrink) within the matrix. Regarding issue (2), in the presence of a fixed gap d the type (a) samples have an absorption coefficient $\alpha = \mu d = \sigma \rho d$, where σ is the absorption cross-section, which is directly proportional to the density ρ. Collection of low-noise spectra with $\Delta \alpha / \alpha \leqslant 10^{-4}$ requires a time stability of the density of the same order of magnitude, which may correspond to a thermal stability requirement of better than ± 0.1 K. These conditions are sometimes difficult to achieve especially for small samples at high temperature. In comparison, the sample absorption geometry (b) is largely unaffected by density fluctuations of the single-sample particles since the average sample density is defined by the matrix volume and does not change. Regarding the third issue the major drawback of type (b) geometry is the increased danger of contamination due to the sample dispersion as compared with case (a) for a bulk sample specimen.

The main experimental techniques and sample environment devices suitable for the collection of x-ray absorption spectra on samples under extreme conditions will be reviewed later in this section. The relevant experimental parameters are the accessible pressure–temperature range and the energy interval for application. The regions of operation of some of these techniques are indicated and compared in figure 2.

2.1. Cells for aqueous solutions

Aqueous solutions at standard pressure–temperature conditions do not generally present serious experimental problems, though cell designs have sometimes been the subject of publication [42]. More challenging experiments are those requiring the application of pressure. As an example, a gas pressure in the range 1–10 MPa is necessary to dissolve a sufficient concentration of noble gas atoms into water for EXAFS measurements of the corresponding (hydrophobic) hydration shell [43] and for this purpose a cell usable up to about 10 MPa and 100 °C was constructed. An improved design was developed at the ESRF [44] able to withstand 100 MPa and 300 °C close to supercritical water conditions. A cell with 2 mm thick silica windows, useful for high-energy edges, was used for solution studies up to 350 °C [45]. Actual supercritical water conditions have been studied with Pt coated Ni alloy cells equipped with synthetic poly-crystalline diamond windows [46].

2.2. Cells for molecular fluids

Chemical reactivity and air sensitivity are the main experimental difficulties for the measurement of most molecular fluids. Cell designs based on polymer windows have been proposed [47]. However, starting from pioneering experiments [10] the use of sealed Pyrex glass or quartz is usually preferred when the window absorption is not critical. A large size flag shaped cell made with 80 μm thick cover glasses and a cylindrical reservoir glued with silicone sealant was found to be suitable for the confinement of liquid Br_2 [48]. A fused silica capillary cell used to measure Mn-containing molecules in supercritical CO_2 has been described [49]. A cell system with Be windows and a 0.6 mm gap used for measuring organic molecules and mixtures in the supercritical fluid state has also been developed [50].

2.3. Autoclave system for high pressure/high temperature

For the previous systems the pressure is held directly by the sample confinement material. In several interesting cases, however, the sample cell, needed to preserve chemical purity, cannot withstand strong pressure differences with the surrounding environment. In these cases,
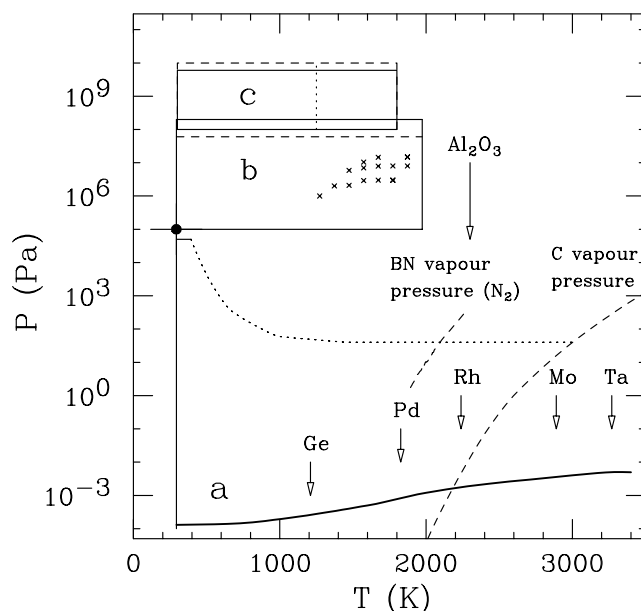
Figure 2. Regions of operation of some of the available experimental techniques for EXAFS under extreme conditions of high temperature and high pressure. The melting points of some elements or compounds (vertical arrows) and the curves (dashed) corresponding to the N_2 vapour pressure of BN and C vapour pressure of graphite are reported. The thick solid line (a) refers to the typical operation of the L'Aquila-Camerino oven using a turbo pumping system. Without additional cooling, the system can operate also with a residual atmosphere up to a pressure roughly indicated by the dotted curve. The region of operation of the autoclave cell of Tamura and co-workers is roughly indicated as region (b). Maximum operating pressures of 80 MPa and 200 MPa are reported according to the vessel size. The maximum operating temperature is limited to about 2000 K by the stability of the sapphire windows. The crosses represent actual experimental points reported in [152]. The typical operation range of the large volume technique using the Paris–Edinburgh press is indicated as region (c). The minimum achievable stable pressure is about 0.1 GPa. Maximum pressures of 6 GPa are normally achieved while higher pressures up to 10 GPa (dashed line) have been exceptionally obtained. The maximum operating temperature is about 1500–1800 K but a direct measurement with a K thermocouple is possible only up to about 1250 K (vertical dotted line).

experiments can still be performed in an autoclave system. The most challenging experimental technique of this kind has been developed by Tamura and co-workers [51] where 5 mm thick Be windows are used in the external cold vessel to hold gas pressures up to 80 or 200 MPa depending on the window design. The sample cell for EXAFS is made of glazed polycrystalline sapphire parts with a central flat gap whose thickness can be made as small as 30 μm and can be heated up to 1900 K. The operation region is reported as region (b) in figure 2. These impressive performances have been widely exploited to study fluid Se in a wide pressure and temperature range around the critical point and through the semiconductor–metal–insulator transition sequence.

A simpler version of this autoclave technique using quartz cells and Al windows able to withstand up to 10 MPa and 700 K was developed by Buontempo [52] for the study of liquid I_2 along the liquid–vapour coexistence curve. In this case the sample cells are made of two 1 mm thick sealed coaxial quartz cylinders. In such a technique, suitable for edge energies above 25 keV, the sample is confined in the gap between the cylinders.

2.4. High-pressure techniques, $P > 0.2$ GPa

The first published high-pressure experiment using EXAFS was performed using a modified Bridgman-anvil method [53] reaching 6.4 GPa on a FeS_2 solid sample. The potential to apply this technique to liquids was addressed. An evolution of the device to allow for x-rays passing along the anvil axis (diamond or B_4C) was later developed [54]. Polycrystalline B_4C anvils are suitable for energy scanning XAS experiments under extreme conditions with an upper pressure limit of about 8–10 GPa.

A wide-aperture high-pressure cell with 3 mm thick Be windows limited to 0.8 GPa with direct compression of the fluids has been also described [55].

The use of a conventional diamond anvil cell (DAC) for high-pressure EXAFS studies is hampered by the presence of sharp Bragg reflections from the diamonds which are seen as absorption peaks. A successful high-pressure technique has been developed by the high-pressure group of LURE [56] for use in conjunction with a dispersive EXAFS facility [57,58]. In dispersive EXAFS the entire spectrum is collected simultaneously with sub-second acquisition times allowing for an effective *in situ* alignment procedure aimed at displacing all Bragg peaks out of the energy region of interest. Under these conditions DACs are usable in the 8–15 keV range attaining pressures up to the 100 GPa range.

2.5. Combining high pressure and high temperature

Investigations of the liquid state of matter at high pressure normally require sample heating. The LURE group has developed an externally heated DAC system suitable for liquid matter investigation. The maximum temperature is limited to about 800 K to preserve the diamonds.

An alternative beautiful technique to combine high pressure and high temperature is based on use of the Paris–Edinburgh press [59] (originally developed for neutron diffraction experiments). The samples are confined in boron-epoxy gaskets which are transparent to x-rays above ≈ 10 keV (for 7 mm gaskets) and are heated through a conductive path with an inner graphite (higher resistance) cylinder. This technique [60] is capable of spanning the region from 0.1 to about 6–10 GPa and up to 1500–1800 K, region (c) in figure 2, with a large freedom in temperature and pressure control. This technique was originally developed at LURE and successively implemented and further developed at the ESRF at the BM29 beamline [61] for EXAFS and at ID30 for x-ray diffraction experiments [62].

2.6. Furnaces and heatable sample holders for EXAFS

Due to the importance of temperature as a parameter for EXAFS, several furnaces or heatable sample holders have been described since the pioneering experiments. Devices suitable for the study of molten materials include a furnace able to operate in vacuum or under controlled atmosphere up to about 1000 K [25, 63] and a cell suitable for the investigation of molten halides up to 1000 °C [64]. Several devices have also been proposed for performing *in situ* investigations of catalytic processes often suitable for combined XAS and x-ray diffraction experiments [65, 66].

A versatile high-vacuum furnace (L'Aquila-Camerino oven) [41], specifically developed for the investigation of liquid matter, has been widely used and is available at several synchrotron radiation beamlines (D42–D44 at LURE and BM29 at the ESRF [61]). The crucible is made using thin x-ray transparent foils (graphite or metallic) in order to achieve an excellent sample temperature homogeneity with a low heat capacity. The typical pressure–temperature range of operation is indicated as region (a) in figure 2, the limiting temperature with graphite crucibles being about 2500 K. Higher temperatures and/or a C free environment

can be obtained with metallic foils. As an example EXAFS measurements of liquid Rh have been performed in a HfO_2 powder matrix and using a W crucible [67].

Other furnaces for high-temperature experiments have been developed by Farge and co-workers, mainly for applications in the geophysical field. These include a system in which the sample is placed in a hole of a $Pt_{90}Rh_{10}$ heating wire, able to reach 2000 K (3700 K in vacuum) [68] and another furnace used for the investigation of silicate melts [69] using fluorescence detection.

2.7. Droplets and powder mixtures, undercooling, temperature-scans and ESXD

The samples suitable for the previous two techniques fall into the powder mixture category previously discussed (figure 1(b)). The first suggestion to measure a stable liquid sample at high temperatures in the form of micron sized droplets mixed in a matrix powder was given to us by Orton who first applied this technique to Ge powder dispersed in BN [70]. This technique was further developed [41] and extensively applied to solid specimens heated above the melting point into the liquid state. Liquid samples in the form of micrometric droplets may be subjected to a deep undercooling due to the volume scaling of the nucleation rate probability. The possibility of preparing a sample in the undercooled liquid state, stable during the time required for XAFS measurements, was first realized in the case of Hg and Ga emulsions [40] and subsequently for Ge [71]. A Japanese group [72] was able to produce Te particles with a diameter in the range 10–100 nm embedded in NaCl or KI by means of evaporation techniques. It was possible to undercool these samples up to about 200 K below T_m.

The occurrence of undercooling in Ge droplets was eventually confirmed using a powerful (and still largely unexploited) x-ray absorption temperature scanning technique [73, 74]. This technique exploits the strong phase contrast existing in the absorption spectrum of a substance, due to structural (and/or electronic) changes at a first-order phase transition. By monitoring the sample absorption coefficient $\alpha(T|E^*)$, as a function of temperature T at a fixed energy E^* (or at a collection of different energy points) it is possible to observe melting (as a discontinuity at T_m) and undercooling as a hysteresis of the $\alpha(T|E^*)$ curves. In a recent paper De Panfilis and Filipponi [75] have shown the possibility to analyse quantitatively the recrystallization part of these hysteresis curves and to obtain a physical measurement of the nucleation rate $I(T)$.

A further experimental complement to the modern x-ray absorption spectroscopy setup concerns the possibility of recording high-resolution powder diffraction patterns of the specimens being investigated, at fixed pressure and temperature. This is achieved using a two-slit collimator in front of a scintillation detector pointing at a fixed angle 2θ on the sample. The k-space scanning is performed through a monochromator energy scan in the desired range. Such an energy scanning x-ray diffraction (ESXD) setup at an EXAFS beamline was first implemented at the ESRF-BM29 [61]. The need to complement EXAFS with temperature scans and ESXD on a single instrument stems from the requirement to implement powerful diagnostic techniques. ESXD is essential to provide a check on the purity of the crystalline components of the sample, to confirm the persistence of undercooling, and to allow for an independent pressure/temperature determination from the equations of state of crystalline calibrants (essential for the large-volume high-pressure technique [61]). All these experimental advances have opened the possibility to design integrated experimental stations for the investigation of the liquid state of matter in thermodynamic equilibrium, but also in the non-equilibrium undercooled state, through a combination of techniques. Recent experiments [76] have also indicated the possibility of producing undercooled liquid samples at high pressure, an occurrence that, if confirmed, would open entirely new fields of investigation.

2.8. Levitation techniques

The wide interest in the measurement of undercooled liquids, possibly also under high-purity conditions, has stimulated the development of containerless levitation techniques for EXAFS. Electro-magnetic levitation [77] was implemented by Egry and co-workers [78] for the study of the EXAFS of undercooled metallic liquids. Due to the large sample size (in the mm range) this technique is not suitable for x-ray absorption detection but requires measurements in the fluorescence mode. These measurements are characterized by a higher noise level and, for concentrated specimens, are affected by non-linear self-absorption effects in the signal. These additional experimental difficulties are an unavoidable price that has to be paid for the measurement of high-purity specimens.

An alternative technique is aerodynamic levitation that, coupled with laser heating, is also suitable for investigating insulating materials. The technique has been developed for x-ray diffraction measurements [79] and also for EXAFS experiments by Landron and co-workers [80].

3. Theoretical framework

The theoretical foundations for the interpretation of the EXAFS phenomenon underwent considerable developments in recent years leading to a theory in substantial quantitative agreement with experiments. Following the publication of a recent exhaustive review on this matter [37] we will confine the present treatment only to general concepts and to the issues more relevant to the field of liquids.

The outline of a modern EXAFS calculation is illustrated here with the intent of highlighting the main approximations by stating their validity and limitations. The x-ray photon–electron interaction is treated to first order in time-dependent perturbation theory leading to the following general expression for the transition rate $W_{i \to f}$ between asymptotic initial Ψ_i and final Ψ_f many electron states

$$W_{i \to f} = \frac{2\pi}{\hbar} \sum_f \left| \langle \Psi_i | \sum_j \frac{e}{m} \boldsymbol{A}(\boldsymbol{r}_j) \cdot \boldsymbol{p}_j | \Psi_f \rangle \right|^2 \delta(E_f - E_i - \hbar\omega). \tag{3}$$

The index j refers to the various electrons in the system each of charge $-e$, mass m, and momentum $\boldsymbol{p}_j$. The photon field $\boldsymbol{A}(\boldsymbol{r}_j)$ is calculated on the position operator of each electron $\boldsymbol{r}_j$. The $\sum_f$ extends over all final states compatible with energy conservation thus accounting for both discrete and continuum spectra.

3.1. Reduction to a one-electron r-space dipole matrix element

The simplification of the previous insoluble many-electron problem into an effective approximate one-electron calculation can be performed according to the following schematic route. To fix the ideas we will consider the case of a Kr atom. The ground state many-electron wavefunction Ψ_i will be approximated by a single-configuration Slater determinant composed of one-electron orbitals obtained from a suitable self-consistent atomic calculation corresponding to the ground-state electronic configuration ($1s^2 2s^2 2p^6 3s^2 3p^6 3d^{10} 4s^2 4p^6$). For the excited state the starting approximation (even if poorer than for the ground state) will also be that of using a single Slater determinant corresponding to the excited state configuration. The relaxation of the electronic charge around the core-hole can be accounted for by adopting a different basis set of self-consistent orbitals [81], optimized for the final state configuration. A typical K-edge excited state configuration is ($1s 2s^2 2p^6 3s^2 3p^6 3d^{10} 4s^2 4p^6 \epsilon p$) in brief [1s]$\epsilon$p

indicating explicitly the core hole and photoelectron in the continuum state of energy ϵ. By expanding all the $N!^2 N$ terms in the N-electron matrix element it is easy to see that the dominant contribution comes from a set of identical terms adding up to

$$\langle 1s|\boldsymbol{A} \cdot \boldsymbol{p}|\epsilon p'\rangle \langle 1s|1s'\rangle \langle 2s|2s'\rangle^2 \langle 2p|2p'\rangle^6 \cdots \; + \; (-1)^{\mathrm{P}}(\text{exchange terms}) \approx \langle 1s|\boldsymbol{A} \cdot \boldsymbol{p}|\epsilon p'\rangle. \quad (4)$$

The label $'$ in the kets indicates that the one-electron orbitals are calculated with a (slightly) different self-consistent potential. As a consequence overlap factors are slightly smaller than 1 and additional terms, in which electrons differing in the principal quantum number are exchanged, do not strictly vanish.

The matrix element can be further simplified by neglecting the spatial variation of the vector potential $\boldsymbol{A}$ (dipole approximation). The validity of the dipole approximation stems from the limited extension of the core electron wavefunction with respect to the wavelength of the photon required to excite it, a condition particularly well satisfied for K-edges. This approximation is, however, not a main limitation of the theory and the inclusion of additional terms in the multi-pole expansion for the transition operator is possible, if necessary, at the expense of a slightly more involved algebra.

Strictly connected with the many-body problem is the possibility of using an r-space representation for the transition operator. This is normally achieved by using the commutation rule $[\boldsymbol{r}, \hat{H}] = \mathrm{i}\hbar/m\hat{\boldsymbol{p}}$. The action of the Hamiltonian $\hat{H}$ on the wavefunctions factorizes a term proportional to $E_i - E_f$. This, however, is strictly correct only when exact wavefunctions (eigenstates of $\hat{H}$) are used. In the present case the straightforward application of this procedure to approximate wavefunctions implies an additional approximation.

After the reduction of the transition matrix element to a one-electron r-space form, and normalizing the absorbed power to the incoming photon flux, we obtain the usual expression for the x-ray absorption cross-section

$$\sigma(\hbar\omega) = 4\pi^2 \alpha \; \hbar\omega \; \sum_f |\langle i|\hat{\epsilon} \cdot \boldsymbol{r}|f\rangle|^2 \delta(E_f - E_i - \hbar\omega) \quad (5)$$

where α is the fine structure constant, $\hbar\omega$ is the photon energy, $\langle i|$ and $|f\rangle$ are the initial (ground state) and final (excited state) one-electron wavefunctions.

3.2. Multi-electron excitations

The approximations outlined in section 3.1 neglect several important many-body effects, and the inclusion of corrections, at least at the empirical level, is required to improve the agreement with experimental data. A first class of effects, usually referred to as 'intrinsic', is that associated with the multi-electron response of the photoabsorber atom.

The previous calculation scheme, in the sudden approximation formalism originally introduced for the theory of x-ray satellites [82], is able to predict non-negligible transition matrix elements to final state configurations in which additional electrons, besides the core level involved in the main edge, are excited. Following the previous example (Kr atom), let Ψ_1 be the many-electron wavefunction (approximated by a single-Slater determinant) corresponding to the final state 'shake-up' configuration ([1s3d]4dϵp) in which an additional 3d electron is promoted to a one-electron state with higher principal quantum number. Owing to the charge relaxation effect and to the resulting non-orthogonality of the wavefunctions with different principal quantum numbers, the transition matrix element in equation (5)

$$M_{i \to \Psi_1} \approx \langle 1s|\boldsymbol{A} \cdot \boldsymbol{p}|\epsilon p\rangle \langle 3d|4d'\rangle \quad (6)$$

does not vanish. The resulting double-electron excitation cross-section is proportional to the main K-edge cross-section times a factor proportional to the squared overlap between the $\langle 3d|$ orbital in the initial state and the $|4d'\rangle$ orbital in the final state.

In addition to these shake-up channels, double electron excitations include discrete resonances, and shake-off transitions where both electrons are ejected. All these transitions contribute to a complex atomic background shape where each double vacancy core-hole state contributes with a sort of scaled replica of the K-edge shifted by the energy required for the additional internal excitation. The intensity of these channels is predicted to be of the order of up to a few % of the main K-edge channel. The 3d $\rightarrow$ 4d' transition in Kr of the previous example is actually observed as a secondary absorption step about 110 eV above the Kr K-edge [43, 83]. A very similar example of double-electron excitation effects will be later illustrated for the Ge case in section 4.4. The existence of background features associated with double-electron excitation channels is well established. These features have been identified in the atomic absorption background of basically all one-electron x-ray absorption edges and in particular in several experiments involving liquid phase samples (due to the weakness of the structural signal) [43, 71, 83–89] and several others. These effects are an integral part of the atomic absorption background, the EXAFS signal is superimposed on this atomic background and the separation between the structural and multi-electron excitation signals is a non-trivial aspect of the data analysis.

Another effect of these intrinsic excitations is to produce an amplitude reduction of the EXAFS oscillation with respect to the one-electron calculation. According to the theory developed by Rehr *et al* [90] the cross-sections of all these channels, including those associated with low-energy excitations, add up with their own shifted EXAFS giving rise to an effective energy-dependent amplitude reduction factor of the EXAFS oscillation $S_0^2(k)$. In practical comparisons between experiments and calculations this effect is usually taken into account by multiplying the theoretical $\chi(k)$ by an empirical constant amplitude reduction factor S_0^2, usually found to be in the range 0.7–0.9. In the data analysis of unknown structures the presence of a normalization factor requires the calibration of the amplitude scale using model compounds.

3.3. Inelastic losses

Another important class of many-body effects, referred to as 'extrinsic', involves the excitation of other electrons in the system (those belonging to neighbouring atoms with localized or extended wavefunctions as occurs in a solid) including collective plasmon excitations. All these inelastic scattering processes destroy the coherence of the excited state photoelectron in such a way that it no longer contributes to the matrix element interference. Such an effect can be accounted for by introducing an empirical effective photoelectron mean-free-path, as in the standard EXAFS formula equation (1), or within a more rigorous formalism [91–93], introducing an effective one-electron potential for the photoelectron corresponding to the denominator of the one-electron Green function in a many-electron system. In the spirit of the local density approximation (LDA) this effective potential is taken as $V(r, E) = V_{\text{Coulomb}}(r) + \Sigma(E, \rho(r))$ where $V_{\text{Coulomb}}(r)$ is the Coulomb potential and $\Sigma(E, \rho(r))$ is the self-energy of an electron travelling in a uniform electron gas of density ρ. This function therefore takes the role of the exchange and correlation potential in a usual low-energy LDA calculation. For high-energy electrons common approximations used for conduction band electrons are not appropriate and a suitable approach was developed by Hedin and Lundqvist [94] resulting in a complex energy-dependent functional form. The energy dependence accounts for the gradual reduction of the exchange potential for high-energy photoelectrons and the imaginary part of the self-energy accounts for the inelastic losses. Several aspects of the implementation of this potential for EXAFS calculations are discussed in the literature [91–93].

3.4. The effect of the surrounding matter

At the level of approximation so far introduced the cross-section is calculated on the basis of one-electron transition matrix elements between a core-wavefunction, calculated from a self-consistent atomic calculation (usually Dirac–Hartree–Fock), and final state wavefunctions calculated in an effective complex potential which includes the Coulomb component (from nuclei and electrons) and an exchange and correlation component in the form of a complex self-energy leading to a non-Hermitian effective one-electron Hamiltonian for the final state.

For an isolated atom the cross-section of the K-edge channel decays smoothly (after threshold) as a function of energy. In the presence of neighbouring atoms the final state potential is modified due to the presence of additional potential wells centred at the surrounding atomic sites R_j, and therefore $V(r) = \sum_j V_j(r - R_j)$. The (EXAFS) interference effect in the cross-section originates from the scattering of the photoelectron wavefunction from these sites. It should be stressed here that for the time-scale of the electronic transition, the atomic nuclei can be regarded as fixed at their instantaneous positions, so that the thermal average of the signal must be calculated *a posteriori* similarly to the average for possible structural disorder. For this reason EXAFS cannot access dynamical properties. Another important aspect is that EXAFS is sensitive to structural properties in a way that is intermediate between neutron diffraction (where the scattering centres are the nuclei) and x-ray diffraction (where the scattering is due to the electronic charge). In EXAFS the scattering is due to the potential that is generated by both nuclei and electronic charges in the system.

A given fixed atom configuration can be used to generate a charge density, a final state potential, and an absorption spectrum. An ensemble average can be performed by a suitable configurational average over all possible atomic positions, leading to a spectrum conceptually comparable to experiment. Such an approach is impractical for at least two reasons. Firstly, the calculation of the three-dimensional wavefunction for a general potential is a complicated computational problem. Secondly, the connection between structure and signal in not straightforward. It is clear that the possibility to exploit the EXAFS method for quantitative structural investigations stems from the availability of a calculation scheme able to simplify the connection between structure and signal, if not even to allow for an inversion procedure able to retrieve the structural information. In this respect the Fourier transformation algorithm [16] is a rather effective procedure since it allows for a structural determination in real space. Subtleties and limitations were extensively discussed by Hayes and co-workers [95].

3.5. Multiple scattering in the muffin-tin approximation

The observation that the photoelectron scattering depends mainly on the inner part of the atomic potential wells $V_j(r - R_j)$, and that, at least for energies well above threshold, it is largely insensitive to the details of $V(r)$ in the interstitial region between the atoms, has suggested the possibility of simplifying $V(r)$ into an approximated form in which spherically symmetric atomic scattering centres are embedded in a constant potential region (muffin-tin approximation). A schematic representation of the effect of the muffin-tin approximation on a one-dimensional potential is illustrated in figure 3. This approximation is at the basis of most present-day practical EXAFS calculations. In this scheme, the atomic scattering properties depend on the atomic numbers and are largely independent of their environment, whereas the structure defines the location of these atomic centres around the photoabsorber atom. This approximation simplifies the cross-section calculation into a (multiple)-scattering problem of the final state atomic wavefunction by a collection of spherically symmetric scattering centres.

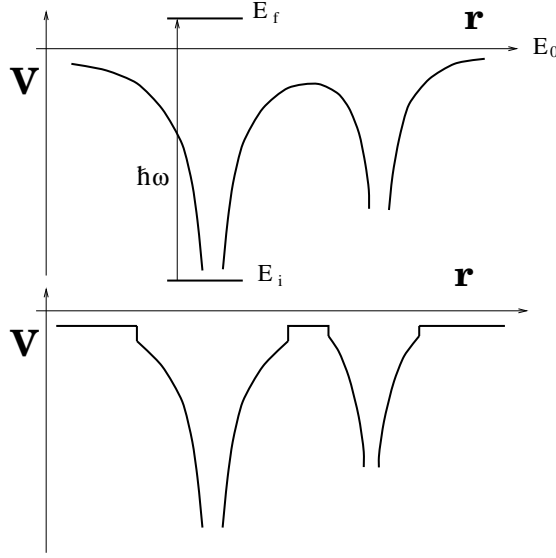Several authors have pioneered the multiple scattering approach for EXAFS calculations

Figure 3. One-dimensional potential curves drawn to give a schematic representation of the effect of the muffin-tin approximation on the effective one-electron potential. The true potential (upper diagram) is substituted by a discontinuous potential (lower diagram) composed of a spherically symmetric atomic potential embedded in a constant potential region. Discontinuities develop at the muffin-tin boundaries. A high-energy photoelectron will be mainly scattered by the inner part of the potential troughs and will not experience a great difference between the two cases.

[96–98], which has been the subject of a previous review article [99]. The photoelectron scattering problem can be solved equivalently [98] in a wavefunction or in a Green function approach. In the latter approach [96] the cross section is rewritten in terms of the Green function for the final state Hamiltonian $G^+(E)$ as:

$$\sigma(\hbar\omega) = 4\pi^2\alpha\,\hbar\omega\,\frac{1}{\pi}\mathrm{Im}\langle i|\hat{\epsilon}^* \cdot r\,'|G^+(E_i + \hbar\omega)|\hat{\epsilon} \cdot r|i\rangle. \tag{7}$$

Useful expressions for the Green function in the case of a collection of spherically symmetric muffin-tins embedded in a constant potential region were previously derived [100]. The multiple scattering formalism has been further developed for the EXAFS case by Natoli, Benfatto, Brouder and co-workers [93, 101, 102].

The polarization averaged cross-section for s core electron (K, L_I, ...) edges (for which the final state angular momentum $\ell = 1$) and the case of real potentials, where the atomic cross-section σ_0 can be rigorously factorized out [93], results in:

$$\sigma(\hbar\omega) = \frac{\sigma_0}{(2\ell+1)\sin^2(\delta_\ell^0)}\mathrm{Im}\sum_m[(\mathbf{I} + \mathbf{TG})^{-1}\mathbf{T}]_{L,L}^{0,0} = \sigma_0\,[1 + \chi(k)] \tag{8}$$

where $\mathbf{I}$ is the unit matrix in the site $0, \ldots, j, \ldots$ and angular momentum $L = (\ell, m)$ indices. The off-diagonal matrix in the site indices $\mathbf{G} \equiv G_{L,L'}^{i,j}(1 - \delta_{i,j})$ describes the free propagation among the sites. The general expression for an off-diagonal site block involves $3J$ symbols and is given by:

$$G_{L,L'}^{i,j} = -[4\pi(2l+1)(2l'+1)]^{\frac{1}{2}}\sum_{l_1}(2l_1+1)^{\frac{1}{2}}\begin{pmatrix} l & l' & l_1 \\ 0 & 0 & 0 \end{pmatrix}$$
$$\times \begin{pmatrix} l & l' & l_1 \\ m & -m' & m'-m \end{pmatrix}(-1)^{m'}i^{l_1+1}h_{l_1}^+(kR_{ij})Y_{l_1,m'-m}(\hat{R}_{i,j}). \tag{9}$$

Here h_l^+ are Hankel functions, $Y_{l,m}$ are the spherical harmonics and $\boldsymbol{R}_{i,j} = \boldsymbol{R}_i - \boldsymbol{R}_j$ the vector joining site j to site i.

Finally the matrix $\mathbf{T} \equiv t_\ell^i(E)\delta_{i,j}\delta_{L,L'}$ is diagonal in the site and angular momentum indices and accounts for the (energy-dependent) scattering properties of the atomic potentials. The generic diagonal t-matrix element for site j, $t_\ell^j = \exp(\mathrm{i}\delta_\ell^j)\sin(\delta_\ell^j)$ represents the effect of the scattering potential on each partial wave of angular momentum ℓ. The energy-dependent function $\delta_\ell(E)$ represents the phase-shift acquired by the solution of the Schrödinger equation going from the origin to the muffin-tin boundary, with respect to the $V = 0$ case.

As a result of the muffin-tin approximation the atomic scattering properties are independent of the actual atomic positions. The distance of the neighbours affects only the phase factor associated with the free propagation of the photoelectron from one atomic centre to another. A wide range of experimental evidence for the validity of the resulting phase and amplitude transferability of the EXAFS signals has already been obtained within the framework of the standard data analysis [103].

3.6. Irreducible n-body signals and configurational average

Equation (8) implies a strongly non-linear connection between structure, defined by atomic positions in the $\mathbf{G}$ matrix, and signal, due to the matrix inversion involved. A consequence of this non-linearity is that the signal cannot be simply decomposed into a sum of pair contributions. In other words, if neighbouring atoms are added progressively, the χ signal with two neighbours is not just the sum of the two independent contributions, since there is an additional (multiple scattering) effect due to the simultaneous presence of both atoms. On the basis of equation (8) it possible to calculate cross sections $\sigma(0, i, j, \cdots)$ associated with a photoabsorber 0 surrounded by an arbitrary number of atoms, and this approach can be used to define and calculate the irreducible n-body contributions to the EXAFS signal [104]. The pair and triplet contributions due to atom i or atoms i, j surrounding the photo-absorber are given by:

$$\gamma^{(2)}(0, i) = \sigma(0, i)/\sigma_0 - 1 = \chi_2^{0i0} + \chi_4^{0i0i0} + O(\chi_6) \tag{10}$$

$$\gamma^{(3)}(0, i, j) = \sigma(0, i, j)/\sigma_0 - \sigma(0, i)/\sigma_0 - \sigma(0, j)/\sigma_0 + 1. \tag{11}$$

These signals are oscillating functions of k with a leading phase equal to $2R_{0i}$ for $\gamma^{(2)}(0, i)$ and $R_{0i} + R_{ij} + R_{j0}$ for $\gamma^{(3)}(0, i, j)$. They can be calculated directly using the above equations which involve matrix inversions, or expanded into the corresponding multiple-scattering series, indicated explicitly in equation (10). For $\gamma^{(2)}$ the leading term corresponds to the well known single-scattering contribution which is given by [105]

$$\chi_2^{0i0}(k) = \mathrm{Im}\left\{\exp(2\mathrm{i}\delta_\ell^0)\sum_{\ell'}(2\ell' + 1)t_{\ell'}^i\sum_{\ell''}(2\ell'' + 1)\begin{pmatrix}\ell & \ell' & \ell'' \\ 0 & 0 & 0\end{pmatrix}^2\left[h_{\ell''}^+(kR_{0i})\right]^2\right\}. \tag{12}$$

This expression is an exact curved wave expression which is at the basis of any modern single-scattering EXAFS calculation. Efficient equations for higher multiple-scattering paths were first introduced by Gurman *et al* [106] and other authors [102].

The total cross-section for a generic fixed atomic configuration surrounding the photoabsorber is then given, to the three-body order, by

$$\chi(k) = \sum_i \gamma^{(2)}(0, i) + \sum_{(i,j)} \gamma^{(3)}(0, i, j). \tag{13}$$

Comparison with real spectra requires the execution of a suitable average over the equivalent photoabsorber atoms and over the effect of the atomic motion (thermal vibration or diffusion)

both of which are accounted for by a suitable ensemble average over the equal time pair (and higher-order) correlation functions. For a monoatomic system described by a pair distribution function $g(r)$ and a triplet distribution $g_3(r_1, r_2, \phi)$ (here r_1 and r_2 are the distances of two neighbours and ϕ the angle centred on the central atom) the ensemble averaged signal is given by

$$\langle \chi(k) \rangle = \int_0^\infty dr\, 4\pi r^2 \rho g(r) \gamma^{(2)}(r, k)$$
$$+ \int dr_1 dr_2 d\phi\, 8\pi^2 r_1^2 r_2^2 \sin(\phi)\, \rho^2 g_3(r_1, r_2, \phi)\, \gamma^{(3)}(r_1, r_2, \phi, k). \tag{14}$$

The present equation is much more general and powerful than equation (1), for the description of the ensemble averaged EXAFS signal. Firstly, the signals are not limited to the single-scattering expression with phenomenological mean-free-path corrections but include multiple-scattering contributions. Secondly, the structural model is not confined to the very special case of a sequence of Gaussian shells and can account for the structure of liquids and glasses.

The importance of the successive contributions to the cross-section decreases with the order, and in several cases most of the signal can be accounted for by the first pair term, especially for disordered matter. There are however several exceptions to this rule and the importance of three-body and higher-order signals has been widely recognized in several cases including ordered and disordered systems. These terms are the direct manifestation of multiple-scattering effects in the photoabsorption cross section. In a sense they are unwanted terms since they complicate the signal, on the other hand they embody a unique valuable characteristic of this spectroscopy namely the sensitivity to higher-order distribution functions [101].

3.7. General considerations

The validity of the present theoretical scheme [104, 107] can be assessed using simple structures characterized by small disorder. The most suitable test systems are clearly isolated molecules and simple crystalline structures at low temperature, where the thermal vibrations can be treated in the harmonic approximation, i.e. assuming Gaussian distribution of neighbours around the average distance R with variance σ^2. The configurational average of the χ_2 terms of equation (12) results in small amplitude and phase corrective factors as will be discussed later for equation (18). Accurate expressions for the configurational average of multiple-scattering terms can be similarly worked out [108]. Simple molecules present the advantage of having a finite number of atomic configurations surrounding the photoabsorber, and, in particular, diatomic molecules represent an ideal test system for the pair contributions. The accuracy achieved with molecules such as Br_2 can be appreciated from previous publications [109]. As expected the present theory with a reasonable choice of empirical parameters S_0^2, E_0, and muffin-tin radii, is able to fully account for the oscillating signal above $k \approx 4$ Å^{-1}, i.e. the region where the muffin-tin approximation is expected to be valid, with structural parameters R and σ^2 coincident within experimental error with the known values.

These kinds of comparison are also useful in order to understand the limitations of the present theoretical scheme. The muffin-tin approximation fails at energies closer to the edge, and a proper non-muffin-tin calculation is required. Several approaches have been followed with promising results [110–113], although the calculation methods are still not available for general use. It has also been pointed out [112] that the use of a self-consistent charge density (as opposed to the superposition of atomic densities) is a necessary improvement to be combined with a non-muffin-tin calculation to achieve improved results.

It is also clear, however, that the muffin-tin approximation is just one of the numerous limitations of the present theory, and that the execution of a non-muffin-tin calculation often

appears not to be the most important improvement required. Many-body effects, and in particular those associated with the opening of double-electron (or multi-electron) excitation channels, generate background anomalies overlapped with the EXAFS. The one-electron atomic cross-section predicted by the above theory is featureless and, in order to compare experimental EXAFS with theoretical calculations, it is necessary to perform a proper atomic background subtraction. The Fourier filtration technique, which is widely used to eliminate the unwanted frequency components of the signal, is inadequate since it hides the problems (at the expense of considerable loss of information) instead of solving them. In fortunate cases it is possible to compare directly free atom and embedded atom spectra [43] and attempt a direct subtraction of the experimental data, but, also in these cases, it is clear that the excitation background is not fully transferable. Attempts to predict background shapes are out of the reach of present theoretical schemes, apart from the prediction of channel onset energies which are calculated on the basis of total energy differences in self-consistent field (SCF) calculations (ΔSCF [81]). Some general empirical rules have, however, been established [114] and empirical background modelling has been successfully used to isolate the structural signal in the framework of a previous data analysis scheme [107] in several cases. This empirical strategy is clearly not fully satisfactory in many respects, but it is certainly better than just hiding what is one of the major limitations in our present understanding of the fine details of x-ray absorption spectra.

4. Analysis methods for disordered matter

In this section we will first confine the discussion to the ensemble average of the leading pair term of the signal expansion. Most of the considerations apply equally to liquids, glasses and amorphous solids. In the multi component case the signal $\langle \chi_\alpha(k) \rangle$, observed at an edge of specie α, is given by the sum of contributions from all species β integrated over the corresponding partial radial distribution functions $4\pi\rho_\beta r^2 g_{\alpha\beta}(r)$ (ρ_β being the average atomic density of specie β)

$$\langle \chi_\alpha(k) \rangle = \sum_\beta \int_0^\infty 4\pi\rho_\beta r^2 g_{\alpha\beta}(r) \, \gamma_{\alpha\beta}^{(2)}(k, r) \, \mathrm{d}r. \tag{15}$$

The pair signal $\gamma_{\alpha\beta}^{(2)}(k, r)$ can usually be approximated by its single-scattering expression equation (12) and, similarly to any other scattering contribution, can be recast into an expression which emphasizes the amplitude and phase dependence as:

$$\gamma_{\alpha\beta}^{(2)}(k, r) \simeq A_{\alpha\beta}(k, r) \, \sin\left(2kr + \phi_{\alpha\beta}(k, r)\right) + O(\chi_4). \tag{16}$$

The total phase (later indicated as ψ) is decomposed into a leading $2kr$ term and a remaining contribution $\phi_{\alpha\beta}(k, r)$ characterized by a very small r dependence (due to curved wave effects). This latter function has a roughly linear k dependence $\phi_{\alpha\beta}(k, r) \sim -2ka$, a being a constant typically of the order of 0.3–0.4 Å, explaining the shifts of the peaks of the Fourier transforms of EXAFS signal with respect to the true values. The amplitude function $A_{\alpha\beta}(k, r)$ in equation (16) includes the functional dependence of the back-scattering factor and the effect of the inelastic losses, resulting in a roughly exponential decay with r. This behaviour is illustrated for the case ($\alpha = \beta = \mathrm{Ge}$) of a Ge–Ge single-scattering contribution in figure 4.

The exponential decay of the signal intensity with r is the main reason for the short-range order structural sensitivity of the EXAFS. For practical purposes the upper integration limit R_{max} in equation (15) is usually taken to be in the range 6–10 Å provided a suitable smoothing window function (half-Gaussian with a 1–2 Å width) is adopted to avoid truncation ripples. Equation (15) is at the basis of calculations of the pair contribution to the EXAFS
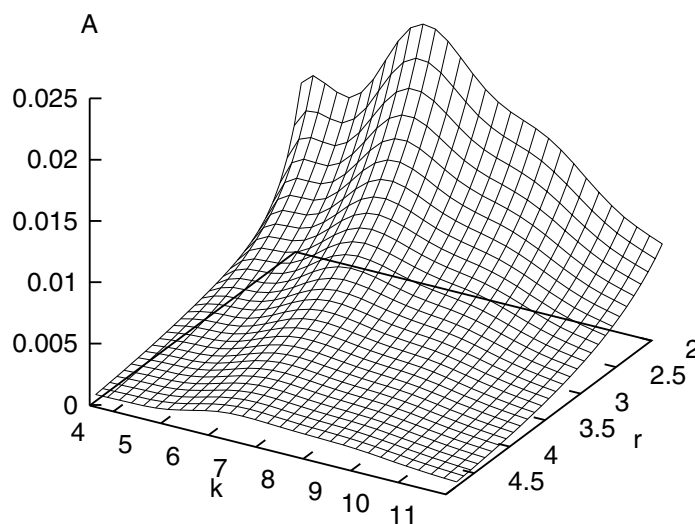
Figure 4. Amplitude $A(k, r)$ of the Ge–Ge χ_2 signal as a function of k (Å^{-1}) and r (Å). The exponential amplitude decay with increasing r, responsible for the short-range sensitivity of the EXAFS, is quite evident from this plot.

signal associated with a given set of partial radial distribution functions. The experimental compatibility between diffraction results and EXAFS can therefore be assessed, integrating the signal over the $g(r)$ determined by diffraction techniques or over the partials, obtained for instance by neutron diffraction through the isotopic substitution technique [115] for a multi-component system. Equation (15) has also been widely exploited for the calculation of the EXAFS signal corresponding to a simulated radial distribution obtained, for instance, by molecular dynamics or Monte Carlo simulations [29, 116, 117].

The solution of the inverse problem, that is, to derive information on the $g_{\alpha\beta}(r)$ from a set of EXAFS spectra is, on the other hand, a rather complicated problem. In the presence of a unique specie of nearest neighbours the averaged signal is found to be dominated by a single-frequency oscillation associated with the first peak in $g(r)$. This occurrence has strongly stimulated scientists to apply a simplified data analysis procedure based on single- (or multiple-) peak fitting, similar to the procedure used for a crystal at high temperature or for a molecule. To account for the increased disorder non-Gaussian model distributions have been adopted. The historical developments and scientific debate on this subject have been rather extensive and the notion of disordered systems has often included crystals at high temperature, amorphous covalent solids, glasses and liquids. The application of the standard EXAFS analysis in the Gaussian approximation was recognized at an early stage to give unphysical results such as an apparent bond length contraction in crystals upon increasing temperature [26, 118]. Several authors have proposed the adoption of non-Gaussian model peak distributions to account for these effects, including an excluded volume model suitable for superionic salts [28], empirical models proportional to $r^2 \exp(-r/l)$ [26] (l is a parameter), or 'physical' models derived from a potential function [118].

4.1. Peak fitting approach

The peak fitting approach is certainly among the most direct and versatile methods for inversion of the structural signal. The partials $g_{\alpha\beta}(r)$ are modelled as the superposition of successive

peaks whose parameters are fitted to the experimental spectrum. The success of this method stems from the ability of the model to mimic the correct shape of the distribution and, from the availability of efficient equations, to calculate the ensemble average of the EXAFS signal over that particular distribution.

A useful four-parameter model function, able to account for asymmetric bond-length distributions, is obtained [71, 116] from a suitably scaled and translated Gamma distribution $f(x) \, dx \approx x^p \exp(-x) \, dx$. The probability of finding one atom at distance r from the photoabsorber is given by the normalized distribution:

$$p(r) = \frac{2}{\sigma|\beta|\Gamma(4/\beta^2)} \left(\frac{4}{\beta^2} + \frac{2(r-R)}{\sigma\beta} \right)^{(4/\beta^2)-1} \exp\left[-\left(\frac{4}{\beta^2} + \frac{2(r-R)}{\sigma\beta} \right) \right] \tag{17}$$

which is defined for $\beta \, (r - R) > -2\sigma$ (with $p(r) = 0$ elsewhere). $\Gamma(p)$ is Euler's Gamma function, calculated for $p = 4/\beta^2$ and defined on the positive real axis. R, σ^2 and β are the three distribution parameters representing the average, variance, and skewness $\beta = C_3/\sigma^3$ (where C_3 is the third cumulant) of the distribution. A fourth multiplicative parameter N can be introduced to represent the average coordination number. The function $Np(r)$ takes the role of $4\pi\rho r^2 \, g(r)$ in equation (15). This functional model was rediscovered several times [119].

Equation (17) is defined for positive and negative β and in the limit $\beta \to 0$ tends to the Gauss distribution. For this reason it represents a very useful model function when an unknown degree of (small) asymmetry has to be fitted. Comparisons with molecular dynamics simulations have shown that equation (17) is a reasonably accurate model of the bond-length distribution in solids [120] and liquids [116]. There is no physical reason for this and any functional model able to describe slight deviations from the Gauss distribution will work as well.

The configurational average of the EXAFS signal over the distribution of equation (17) can be calculated in closed form and expressed in terms of the oscillation amplitude $A_0 = A(k, R)$, the phase $\psi_0 = \psi(k, R)$, and their first and second derivatives with respect to r calculated for $r = R$, ($A_1 = \partial A(k, r)/\partial r|_{r=R}$, and $\psi_1 = \partial\psi(k, r)/\partial r|_{r=R}$ and similarly for A_2 and ψ_2) we find:

$$\langle \chi(k) \rangle = \text{Im}\left\{ A_0 \, \exp\left[i\psi_0 - \frac{4}{\beta^2} \left[\ln\left(1 - i\frac{\sigma\beta\psi_1}{2} \right) - i\frac{\sigma\beta\psi_1}{2} \right] \right] \right.$$
$$\left. \left[1 + i\frac{A_1}{A_0} \frac{\psi_1\sigma^2}{(1 - i\frac{\sigma\beta\psi_1}{2})} + \left(\frac{A_2}{2A_0} + \frac{i\psi_2}{2} \right) \sigma^2 \frac{(1 - \psi_1^2\sigma^2)}{(1 - i\frac{\sigma\beta\psi_1}{2})} \right] \right\}. \tag{18}$$

This and similar expressions are very useful in a fitting procedure since they account for the configurational average through parameter dependent phase and amplitude corrections with respect to the undamped signal $\text{Im}\,[A_0 \exp(i\psi_0)]$ (corresponding to $p(r) = \delta(r)$). They are based on a low-order Taylor expansion for amplitudes and phases around the average distance value R [108] and therefore cannot be used for very broad distributions, wider than about 1 Å.

In the Gaussian limit, obtained for $\beta \to 0$, equation (18) provides a damping factor which is more accurate then just the conventional Debye–Waller factor $\exp(-2k^2\sigma^2)$. The usual Debye–Waller factor can be obtained by assuming $\psi_2 = A_2 = A_1 = 0$, therefore retaining only the leading phase correction term $\exp(-\sigma^2\psi_1^2/2)$, with the additional substitution $\psi_1 = 2k$.

A rather obscure procedure that is widely encountered in the literature consists of highlighting the leading r dependence in the amplitude $A_0(k, r) \approx a_0(k) \, r^{-2} \exp(-2r/\lambda)$ and considering it as a part of $p(r)$ introducing what is usually referred to as an effective distance distribution $p_{eff}(r) \simeq p(r) \, r^{-2} \exp(-2r/\lambda)$. The physical basis behind this approach is in the emphasis on the short-range sensitivity of EXAFS, which is thought to be generated by

$p_{eff}(r)$ rather than by $p(r)$. There are, however, major disadvantages associated with this way of separating the contributions in equation (15). Firstly, the exponential mean-free-path expression is just an empirical correction term, strictly speaking λ is, in general, k and path dependent, and its actual functional form depends on the theory used to calculate the EXAFS. The results of this partition are therefore inadequate since they mix well defined structural unknowns with theory-dependent functional forms and should be discouraged. From the practical point of view, fitting peak shapes in $p_{eff}(r)$ requires correction terms for comparison with real distance distributions.

4.2. The cumulant expansion

The main drawback of the peak fitting approach is in the requirement for certain assumptions about the structural model. While it is true that the validity of these assumptions can be assessed on statistical grounds it is also true that the availability of a model-independent method is desirable. Several true and false model-independent methods have been proposed for EXAFS data analysis. The most controversial example of these methods is certainly the so called 'cumulant expansion method' [121]. In this approach, applicable in the presence of an isolated peak described by a probability density $p(r)$, the average of the phase term in equation (16), written as a complex exponential, can be expanded using the cumulant expansion for the characteristic function as:

$$\langle \exp(\mathrm{i}\,2kr) \rangle \simeq \exp\left(\mathrm{i}\,2k\,C_1 - \frac{1}{2}(2k)^2 C_2 - \mathrm{i}\,\frac{1}{3!}\,(2k)^3\,C_3 + \frac{1}{4!}\,(2k)^4\,C_4 \cdots \right) \tag{19}$$

where $C_1 = R$, $C_2 = \sigma^2$, $C_3 = M_3$, $C_4 = M_4 - 3(\sigma^2)^2$, ..., and M_k is the kth moment about the mean. It is therefore found that even and odd cumulants affect the amplitude and phase of the signal separately appearing in even or odd power series of k. In addition to the possible use of these power series in a peak fitting approach this cumulant analysis has been widely applied directly to the experimental data first by extracting the experimental amplitude and phase function from a Fourier filtration procedure and successively by fitting suitable power series to the phase and log amplitude functions. Even more accurate results can be achieved by using an experimental reference such as an equivalent system at low temperature (where the Gaussian limit is approached) thus obtaining the differences of the cumulants with respect to the reference. This procedure has been widely developed by Fornasini and co-workers [122] for the case of crystalline or amorphous solids. The cumulant expansion method has, however, also been used in the case of highly disordered systems and for liquids. In this latter case it is not clear how the method can be applied at all since the system is characterized by a continuous distribution of distances which produce a long-range tail and the moments of the distribution cannot even be defined!

There are also other general concerns about the application of this method. Firstly the fitting of several successive cumulants becomes rapidly unstable due to the strong statistical correlations among odd (or even) cumulants. Truncating the series at any order higher than the second (which corresponds to the Gaussian limit) is somewhat arbitrary as it does not correspond to any physical distribution. As an example, if only a small correction to the Gaussian limit is required it is possible to fit a value for C_3, which is usually > 0. The r space distribution associated with a positive C_3 can be readily calculated by Fourier transformation and it is found that it is asymmetric but is not positive definite as any probability density should be. Typical examples of the normalized probability densities $f(z)$, assumed in the averaging procedure of equation (19), for different values of $\beta = C_3/\sigma^3$ and $\gamma = C_4/\sigma^4$ are illustrated in figure 5 as a function of the standard random variable $z = (r - \langle r \rangle)/\sigma$. For positive C_4 terms the inverse Fourier integral is not even convergent. So the results of the cumulant expansion

analysis are often difficult to interpret and sometimes not even associated with any reasonable distribution. In conclusion it is my opinion that there is no reason why the cumulant expansion method should give better results than the peak fitting approach.
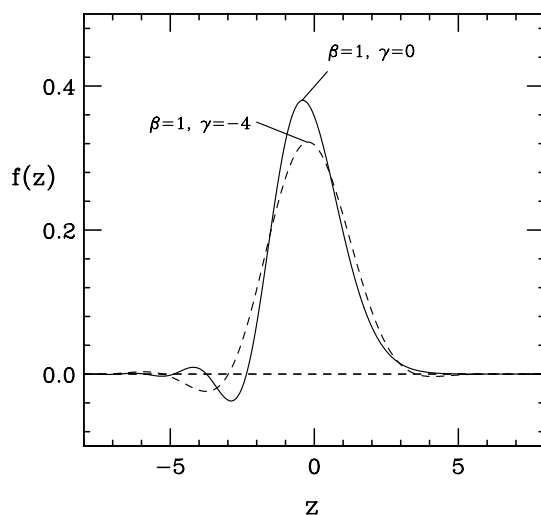

Figure 5. Examples of one-dimensional standardized distributions with $\langle z \rangle = 0$, $\sigma^2 = \langle z^2 \rangle = 1$, $\beta = C_3/\sigma^3 = 1$, and $\gamma = C_4/\sigma^4 = 0$ (solid curve) or $\gamma = -4$ (dashed curve), and vanishing higher-order cumulants, as obtained by Fourier transformation. These functions are not positive definite and therefore they are not useful model functions to represent atomic distributions.

4.3. Fitting $g(r)$ and physical constraints

One of the major drawbacks of both the peak fitting and cumulant expansion methods for liquids is in the assumption of a radial distribution function composed of isolated peaks. While this assumption is realistic for crystals or molecules, in a liquid, even when a strong first-neighbour peak exists, we are in the presence of a continuous distribution of distances starting from the hard-core repulsive limit of the potential and approaching the $g_{\alpha\beta}(r) = 1$ limit for $r \rightarrow \infty$. To such an atomic distribution the concept of cumulant expansion cannot be applied. However, due to the short-range sensitivity, the signal appears not too dissimilar from that of an isolated shell of atoms, and actually a peak fitting analysis is often successful with a single shell of neighbours. The results of this analysis are, however, not necessarily correct and in most known cases the resultant coordination numbers are under-determined.

It is important to stress here that this apparent failure of the EXAFS technique should not be attributed to a real inadequacy of this spectroscopy to investigate the structure of liquids, but rather to the adoption of a wrong data analysis strategy. The main reason for the failure is in the strong correlation between the coordination numbers, widths and shape parameters of the model distributions. In the absence of constraints, very similar signals can be simulated using apparently different parameter choices. In particular small coordination numbers can be fitted with sharper distributions. It is clear that the use of additional information on a system to provide constraints is particularly important.

A fundamental constraint that is often ignored in the analysis of a multi-component system is the symmetry upon exchange of atomic types $g_{\alpha\beta}(r) = g_{\beta\alpha}(r)$. In the peak fitting approach this results in a coordination number constraint. By defining the coordination number of species

β around α as $N_{\alpha\beta} \sim g_{\alpha\beta}(r)\rho_\beta$ we get $N_{\alpha\beta}\rho_\alpha = N_{\beta\alpha}\rho_\beta$, in other words the coordination numbers of mixed bonds seen from the two atomic sites at the different ends of the bond must scale as the number density (or atomic fraction) of the neighbour type atoms. It is a matter of fact that this simple rule is often ignored in the analysis of binary alloy spectra.

A simple but rigorous method to introduce physical constraints into a peak-fitting approach has been proposed by the author in 1994 [123] for a single-component system. As in any other approach based on peak fitting, this procedure is model dependent. However, in this case the distribution is a realistic $g(r)$ model and is not just composed of one (or a few) isolated peaks. The starting $g(r)$ model can be inspired by computer simulation, previous diffraction measurements, or just calculated from very simple interaction potentials (for instance hard spheres). This model is supposed to supply a $g(r)$ with the correct long-distance behaviour, namely $\lim_{r\to\infty}g(r) = 1$ and a correct compressibility limit

$$\lim_{k\to 0} S(k) = \lim_{k\to 0} 1 + \frac{4\pi\rho}{k} \int_0^\infty (g(r) - 1)r \sin(kr)\mathrm{d}r = 1 + 4\pi\rho \int_0^\infty (g(r) - 1)r^2\mathrm{d}r = \frac{\rho K_T}{\beta} \tag{20}$$

where K_T is the isothermal compressibility and $\beta \equiv (k_B\, T)^{-1}$. The $g(r)$ will then be refined in such a way to modify its short-range shape to which EXAFS is strongly sensitive, while maintaining unchanged these (EXAFS insensitive) limits of the corresponding $g(r)$ and $S(k)$. The change in $S(k)$ associated with a change $\Delta g(r)$ in $g(r)$ can be expanded in a Taylor series about $k = 0$ as

$$\Delta S(k) = 4\pi\rho \int_0^\infty r^2 \Delta g(r) \frac{\sin(kr)}{kr}\mathrm{d}r \approx 4\pi\rho \int_0^\infty r^2 \Delta g(r) \left[1 - \frac{k^2}{2!}\frac{r^2}{3} + \frac{k^4}{4!}\frac{r^4}{5} + \cdots \right]\, \mathrm{d}r. \tag{21}$$

The $k \to 0$ behaviour of the $S(k)$ can then be maintained imposing zeroth-order (or even higher) constraints of the type

$$\left(\left. \frac{\partial^{2m}\Delta S(k)}{(\partial k)^{2m}} \right|_{k=0} \right) = 0 \qquad \leftrightarrow \qquad 4\pi\rho \int_0^\infty r^{2+2m}\Delta g(r) = 0 \tag{22}$$

which correspond to even moments of the change in the matter distribution about $r = 0$.

These constraints can be in practice implemented as follows. The initial model $g(r)$ is decomposed into one (or more) short-range peaks plus a long-range tail. To fix the idea two peaks will be considered in such a way that:

$$4\pi r^2 \rho g(r) = N_1\, p_1(r|R_1, \sigma_1^2, \beta_1) + N_2\, p_2(r|R_2, \sigma_2^2, \beta_2) + 4\pi r^2 \rho g_t(r). \tag{23}$$

Owing to the linearity of the pair term the EXAFS signal will be calculated summing the three contributions separately. The tail contribution is calculated by direct integration of equation (15) and is kept fixed. The contributions from peaks 1 and 2 are instead calculated using suitable equations for isolated peaks such as equation (17) which are functions of the corresponding peak parameters. The refinement of the peak parameters is then performed with the following constraints, resulting from equation (22) for $m = 0$ and $m = 1$:

$$\begin{cases} N_1 + N_2 = N^{tot} \\ N_1(R_1^2 + \sigma_1^2) + N_2(R_2^2 + \sigma_2^2) = M_2^{tot} \end{cases} \tag{24}$$

where N^{tot} and M_2^{tot} are the total coordination number and total second moment of the matter distribution about $r = 0$ associated with the two short-range peaks.

The success of the method, which has been widely used in recent years, stems from its simplicity. The method should be regarded as the correct way to generalize the peak fitting

approach to the EXAFS data analysis for liquids and disordered matter. The long-range nature of the atomic distribution in a liquid modifies the data analysis introducing a fixed contribution (from the long-range tail) and constraints involving peak parameters and coordination numbers. These constraints still allow for a redistribution of the coordination environment around the photoabsorber but prevent the fit from assuming unphysical values. In such a two-peak plus tail model with two constraints the number of free parameters is six.

4.4. An example of data analysis

A very instructive example of data analysis, which illustrates the importance of the various contributions to the EXAFS signal in the case of liquids, is the one of elemental Ge [71]. In this subsection the key features of the analysis are reviewed emphasizing the comparison among different methods. The previous analysis [71] is applied to new (Ge K-edge) data for liquid Ge at $T = 1220(5)$ K collected at the ESRF BM29 beamline [61]. Details regarding sample preparation and characterization are similar to those previously described [71, 73, 74]. The data analysis when applied to c-Ge room temperature data yields as first-shell parameters $R = 2.4498(8)$ Å and $\sigma^2 = 0.0035(1)$ Å^2 in perfect agreement with the known structure and vibrational properties of the crystal. The analysis of this reference structure is important to determine the optimal values of the empirical theory parameters such as muffin-tin radii, S_0^2, and E_0 [71].

The raw x-ray absorption spectrum of liquid Ge at the Ge K-edge, magnified in the region between 11.15 and 11.7 keV, is reported in figure 6. A linear background was subtracted from the data, for graphical purposes, and the corresponding difference signal $\Delta\alpha$ is reported in units of the main K-edge absorption discontinuity. The experimental spectrum is duplicated for a better comparison with two different atomic background model functions. In the upper diagram of figure 6 the solid line corresponds to a typical polynomial spline (composed of two third-degree polynomials) used for the EXAFS extraction. The experimental signal is clearly anomalous with respect to the ideal oscillating behaviour of structural origin, and, in particular, it shows a characteristic kink on the maximum of the second EXAFS oscillation, at $E \approx 11\,243$ eV, which results also in an apparent amplitude reduction. This feature is assigned to the opening of double-electron excitation channels involving the simultaneous excitations of the 1s and 3p electrons ([1s3p]) in Ge. The lower diagram of figure 6 reports a more complicated model background function which accounts for all double-electron excitation features labelled as [1s3d], [1s3p] and [1s3s]. The latter was neglected in the previous investigation [71]. The background function of figure 6 (lower diagram) is an empirical model refined together with the structural contribution to fit the experimental signal. The steps are, in this case modelled as arctangent functions depending on amplitude, position of the inflection point and width. The widths of the [1s3p] and [1s3s] arctangents were constrained to be the same, for a total of eight additional background fitting parameters. These parameters are largely uncorrelated with the structural ones since they generate completely different signals. It should be remarked that the intensity of the double-electron excitation features is very small $\Delta\alpha \approx 5 \times 10^{-3}$ for the [1s3p] edge. However, owing to the minuscule (comparable) intensity of the EXAFS signal (a rather general case for liquids) an account of these features is mandatory.

The improvement in the extraction of the EXAFS oscillations and in the fitting, due to the empirical double-electron excitation background, is illustrated in figure 7. In the left-hand panel of figure 7 the experimental (dots) and model $k\chi(k)$ signals (solid curves) obtained using different data analysis methods ((a), (b) and (c)) are compared. In the right-hand panel of figure 7 the corresponding structural results are compared directly on the $g(r)$ scale with previous neutron diffraction [124] results and *ab initio* computer simulations [125].
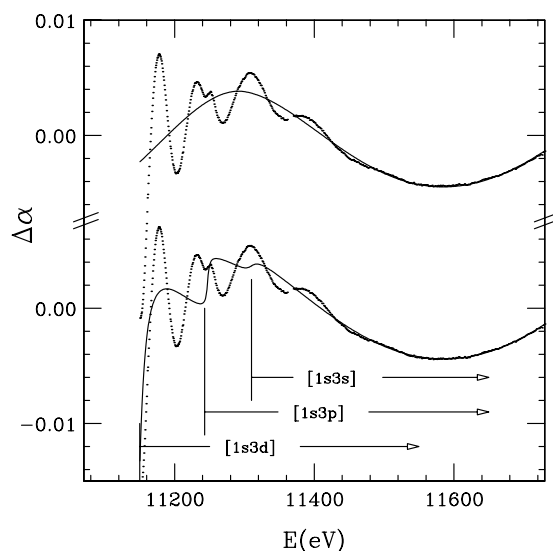
Figure 6. Magnified experimental Ge K-edge spectrum of liquid Ge (dots) and comparison with different atomic background model functions (solid lines). The upper curve is a typical polynomial spline composed of two third-degree polynomials; the lower curve is a complex background model accounting for the successive opening of three double-electron excitation channels labelled as [1s3d], [1s3p], and [1s3s]. The steps are, in this case, modelled as arctangent functions. The [1s3d] feature is visible in the experimental spectrum as a major absorption increase. The step associated with the [1s3p] channels appears as a kink on top of the second EXAFS oscillation. The weaker [1s3s] step is visible only in these high-quality data after subtraction of the structural signal. For graphical purposes the spectra are reported as differences with respect to an average linear absorption decay $\Delta\alpha$ in units of the main K-edge absorption discontinuity.

In the case of model (a) a simple polynomial spline was used for the background. As a result, the experimental EXAFS signal (a) is irregular and cannot be fitted by any physical oscillation. In this case the fitting is largely unstable and remarkably different results can be obtained according to the fitting range and weights. Instead, in cases (b) and (c), the improved background model (corresponding to the lower diagram of figure 6) results in a much more regular oscillation that can be easily modelled by the theory.

In cases (a) and (b) the structural model was composed of an isolated asymmetric peak according to equation (17), whereas in case (c) the fitting was performed according to the procedure described in section 4.3. The most surprising result of this comparison is that an almost perfect fit of the experimental signal is achieved in both cases (b) and (c), using completely different structural models. In case (b) the signal is fitted by an isolated shell of neighbours with coordination number $N = 1.79$, average distance $R = 2.60$ Å, variance $\sigma^2 = 0.024$ Å^2 and a slight asymmetry $\beta = 0.37$. The coordination number is largely underestimated and the peak accounts only for part of the rising edge of the $g(r)$. The inadequacy of this structural analysis based on a peak fitting over a $g(r) = 0$ background is clearly illustrated by this example. In addition, here we understand the danger of such an approach for a liquid/disordered system, since the wrong model is perfectly able to account for the experimental signal.

In case (c) the signal from a realistic $g(r)$ is obtained by adding three contributions (corresponding to two short-range peaks and a tail $g_t(r)$ function). The initial model was taken to be close to the computer simulated $g(r)$ [125]. Of the initial decomposition only
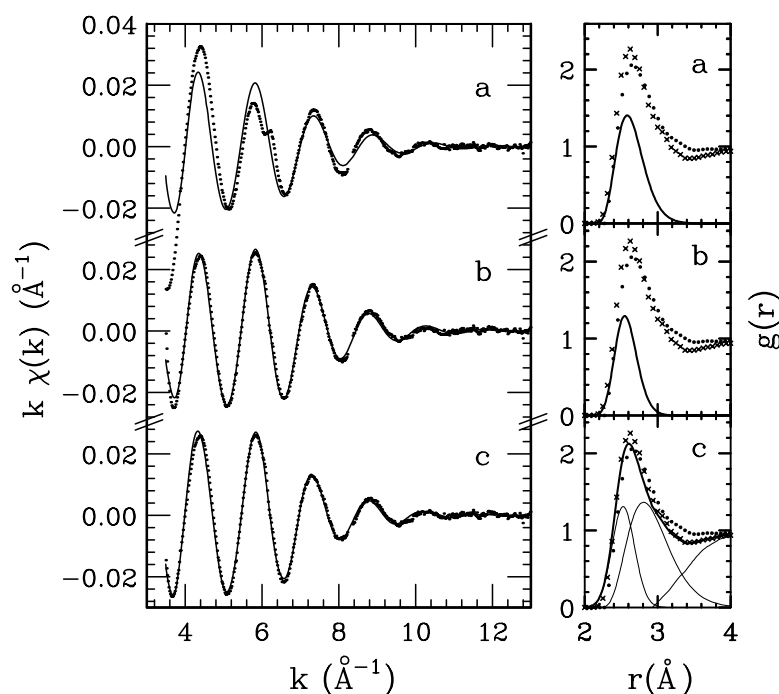
Figure 7. Comparison of different data analysis procedures applied to the liquid Ge K-edge spectrum. In the left-hand side panel the experimental (dots) and model $k\chi(k)$ signals (solid lines) obtained using procedures (a), (b) and (c) are reported. On the right-hand side panel, the corresponding structural results (thick solid lines) are compared directly, on the $g(r)$ scale, with previous neutron diffraction (●) results [124] and *ab initio* computer simulations (×) [125]. The number density is taken as ρ 0.0456 atoms Å^{-3}. Data analysis procedures differ as follows. (a) Atomic background modelled as a simple polynomial spline (upper diagram in figure 6), single-shell peak fitting. (b) Atomic background accounts for double-electron excitations (lower diagram in figure 6), single-shell peak fitting. (c) Atomic background accounts for double-electron excitations as in (b), constrained $g(r)$ refinement; the three $g(r)$ components (two peaks and tail) are reported as thin solid lines. In both cases (b) and (c) an excellent fitting of the experimental signal is achieved, but only in case (c) is the atomic distribution realistic. Analysis (b) is wrong because it is based on a peak fitting with respect to an unphysical $g(r) = 0$ background.

the tail part $g_t(r)$ and the constraints of equation (24) were retained. The model $g(r)$, refined in its short-range part, resulted in a function slightly closer to the neutron diffraction determination [124]. The three individual components in r space, corresponding to the decomposition of equation (23) are reported as thin solid lines on the right-hand panel of figure 7 (panel (c)). The corresponding EXAFS signals are not reported for simplicity; they are not too dissimilar from those of figure 16 in reference [71].

With this method a reliable analysis of the EXAFS spectrum of liquid Ge is performed yielding a $g(r)$ function perfectly compatible with present structural knowledge. Up to about 2.8 Å the present EXAFS result of figure 7(c) is actually a very precise determination of the short-range $g(r)$ shape of liquid Ge. For $r > 3$ Å the $g(r)$ curve is mostly defined by the initial model and cannot be determined by the EXAFS signal.

The comparison of the different data analysis methods should have convinced the reader that the results of several previous EXAFS investigations of liquid/disordered systems based on the fitting of isolated peaks should be taken with caution. In most cases coordination

numbers might have been largely underestimated. Another important aspect in the evaluation of previous research is the type of atomic background adopted to isolate the EXAFS data. In many previous investigations the background subtraction was performed using a simple polynomial spline. A better apparent agreement (between experimental and theoretical data) than the one of our example of figure 7(a) is often achieved by applying a Fourier filtration procedure. It is clear that in those cases the errors of the structural results include also the effects of the wrong background shape that propagate through Fourier filtering, thus adding further uncertainty.

4.5. Other methods

Several model independent approaches have been proposed for EXAFS data analysis in the case of liquid and disordered systems. As pointed out by Babanov and co-workers [126, 127] the inversion of equation (15) is an ill posed problem with a well behaved solution only in the framework of a regularization scheme. This method has been applied to EXAFS and to a combination of techniques, including anomalous x-ray diffraction, and in principle should be able to provide realistic radial distributions functions if used for the EXAFS analysis of liquid systems.

The inclusion of physical constraints on the $g(r)$ imposed by the existence of a realistic three-dimensional distribution of atoms finds its natural implementation in the reverse Monte Carlo (RMC) technique originally developed by McGreevy and Pusztai [128] for the analysis of diffraction data. RMC has also been proposed for the analysis of EXAFS data [129] and exploited also by other authors [130]. In the opinion of the author RMC represents a very valuable approach that is worth investigating further.

4.6. EXAFS and pair potentials

The possibility of gaining insight into the interatomic potentials from the analysis of the EXAFS, owing to its short-range sensitivity, was first addressed in a clear way by Hayes and Boyce [29]. The relationship between (pair) potential and structure is a basic (solved) problem in the framework of statistical physics, as described in textbooks. Quite accurate comparisons between neutron diffraction measurements and calculations can be at present performed for simple fluids [131]. At present (unfortunately) similar insight cannot be obtained from EXAFS. However, it should be kept in mind that the correct reproduction of the observed EXAFS signal puts severe constraints on the short-range part of the potentials used in computer simulations of the corresponding liquid structures.

The comparison of the experimental and simulated EXAFS signal resulting from the atomic distributions simulated through molecular dynamics (MD) or Monte Carlo computer simulations is becoming a very popular practice. Classical ensemble distributions for both liquids and solids at relatively high temperatures can easily be simulated using the previous techniques, while low-temperature vibrational properties of a solid or a molecule can be calculated using the path-integral effective-potential method as recently illustrated by Yokoyama [132]. The simulated distributions $g_{\alpha\beta}(r)$ can be used to calculate the corresponding EXAFS signal on the basis of equation (15), which is perfectly adequate.

A wrong connection between inter-atomic potentials and pair distribution functions has been pursued in several EXAFS papers (not cited here) that we feel important to emphasize. Several authors after deriving experimentally the first-neighbour distribution $p(r)$ calculate what has often been called the 'EXAFS (effective) pair potential' as $u_2(r) \approx -k_B T \ln(p(r))$. It is clear that, even in the assumption of the existence of a pairwise additive potential depending

on the atomic distance $V_2(|r_i - r_j|) = V_2(r)$, for a general three-dimensional system, the probability density of finding two neighbours at distance r is, in general, not proportional to $p(r) \approx \exp(-V_2(r)/(k_B T))$. The proportionality sign is strictly valid only for a two-atom system in one dimension and in the classical high-temperature limit. By no means does the proportionality sign hold for crystals even in the harmonic approximation. As a consequence, in general $V_2(r)$ and $u_2(r)$ are different functions, and the introduction of the latter, which is physically meaningless, can be largely misleading.

4.7. Higher-order distributions

One of the most appealing feature of EXAFS is its potential sensitivity to higher-order (and in particular three-body) distribution functions through the presence of multiple-scattering signals. This presence is well established for crystals and molecules [107] where characteristic signals associated with $n \geqslant 3$-body configurations have been clearly identified and analysed, extracting information on the geometry and correlated vibration of the n-atom cluster. In liquids three-body contributions have often been identified, but additional improvements to the data analysis schemes are required to perform a quantitative analysis.

In a monoatomic close packed liquid the smallest possible three-body configuration is an equilateral triangle between first neighbours. Triplet distributions of simple liquids present a peak for this configuration and this peak, similarly to the first-neighbour peak of $g(r)$, is expected to generate a signal. The triangle perimeter is $3R_1$ giving rise to a leading phase term which locates it at 1.5 times the frequency of the first shell pair signal. In order to identify this signal it is necessary to account correctly for all of the pair signal at that frequency which overlaps and interferes with the possible three-body signal. It is therefore clear that a prerequisite for highlighting three-body contributions is the ability to make an accurate analysis of the pair contributions. In the light of what has been described in this section it could be thought that this is quite a hard task. This is, however, not necessarily the case, since these triplet contributions can often be associated with a precise frequency which does not have any counterpart in the pair-signal and therefore they may appear even in the Fourier transform of the experimental data.

The most promising cases are those in which a clear atomic configuration exists in the liquid as in the case of O–metal–O atom contributions in the first hydration shell of strong electrolytes [101, 133]. Recently, strong multiple-scattering contributions have been observed and analysed in Rb^+ and Sr^{2+} acetonitrile solutions [134].

Other systems where the pair-analysis was insufficient to describe the signal and triplet-contributions were likely to be present include polyvalent metals like Ga especially in the undercooled range [135].

It is clear that this feature of the EXAFS spectroscopy represents one of the areas for major future development. Improvement of data collection and data analysis procedures will open new fields of investigation and allow for novel comparisons with theoretical predictions of the structure of liquids.

5. Applications and main results

In this section the main scientific applications of EXAFS spectroscopy to the liquid state of matter will be reviewed. Most of this work exploits the previously described experimental techniques and data analysis methods. Applications to glasses and amorphous materials are not covered by the present review, and the reader can refer to the extended literature in the field [36, 136, 137].

5.1. Noble-gas fluids

Noble gas fluids are attractive for the possibility of performing very detailed comparisons with the predictions of accurate potential models [131]. The spectra of high-density fluid Kr were measured using the DAC technique at a dispersive EXAFS facility [56] at room temperature in the pressure range 0.1–0.75 GPa (and also in the solid phase at higher pressures) [138]. The spectra were compared with the EXAFS calculated from $g(r)$ functions obtained by means of Monte Carlo simulations in the (N, P, T) ensemble [138]. A very weak structural signal was revealed in agreement with calculations within the experimental error. From these types of experiment, however, it appears evident that, due to the large bond distances involved and large disorder, it is not really possible to improve our knowledge of the Kr–Kr interaction from the EXAFS analysis of liquid phase data. The situation is quite different for the case of solid Kr at higher pressures.

5.2. Elemental liquid metals—undercooling

Following the pioneering investigation on liquid Zn [26] low melting point metals have been widely investigated with the double aim of understanding how the EXAFS sees the liquid environment around the photoabsorber atoms and of improving and assessing data analysis techniques.

A comparison between solid and liquid Sn at the K-edge [139] was interpreted in terms of a substantial survival upon melting of the local coordination environment existing in the solid. In a subsequent investigation of solid and liquid Pb [140] a complex background removal procedure was adopted to increase the available k range for analysis. The presence of strong double excitations of 5p electrons around $k = 6$ Å^{-1} were, however, not identified and the analysis was performed using a single-peak analysis in the cumulant expansion approach resulting in a large apparent decrease of the coordination number in the liquid. The authors explain these results invoking the role of diffusion and a substantial EXAFS blindness to diffusing atoms. While this paper was certainly addressing interesting issues, some statements may appear misleading and the complicated analysis approach may give the false impression that EXAFS cannot provide any valuable information on liquids. The apparent decrease of coordination number is just a consequence of the inadequate data analysis. EXAFS is sensitive to $g(r)$ in the way described extensively in this review and it cannot distinguish between atoms residing in the first shell of neighbours or those which are instantaneously at the same distance but will diffuse away at later times.

In a more recent study, liquid Sn has been re-investigated [141] through a simultaneous analysis of the three spectra collected at the L edges. Structural results in the framework of the constrained peak fitting approach [123] were able to improve the x-ray diffraction determination of the liquid Sn $g(r)$ and provide evidence for three-body contributions from tetrahedral coordination.

Higher melting point simple metallic liquids have been studied more recently using the droplet technique. An experimental comparison between the x-ray absorption spectra of solid and liquid Ag was reported [73]. The structure of liquid Rh has been determined for the first time in an EXAFS experiment [67]. Liquid Pd in an Al_2O_3 matrix has also been the subject of a complete structural investigation [142] aimed at highlighting subtle structural differences between the equilibrium and undercooled liquids. This research [75, 142, 143] is a beautiful example of how modern experimental setups [61] can be used to combine temperature scans (to provide evidence for undercooling and to measure the nucleation rate of crystallization [75]), ESXD (to confirm the absence of crystallization in the undercooled

liquid phase and to characterize sample purity [143]), and XAFS [142] to gain a deep physical insight in the system being investigated and to solve difficult experimental problems.

5.3. Metallic alloys and undercooling

A German group has pioneered very interesting research on undercooled Co–Pd metallic alloys. This system is magnetic and the difference between the liquidus and the Curie temperature reaches a minimum around the $Co_{80}Pd_{20}$ alloy composition, as a consequence of which a deeply undercooled melt may manifest ferromagnetic properties. Deep undercooling can only be achieved by using containerless levitation techniques such as electromagnetic levitation [77] which has been developed and exploited to perform EXAFS measurements on this very interesting alloy [78, 144]. Co K-edge fluorescence measurements on the $Co_{80}Pd_{20}$ molten alloy have been collected to 300 K below T_m and interpreted quantitatively in terms of Co–Co and Co–Pd nearest neighbours [144].

For glass forming metallic alloys it is possible to quench the system into a metallic glass and access the undercooled liquid region from the low-temperature side prior to crystallization. An EXAFS investigation on the temperature transformation of the $Zr_{65}Al_{7.5}Cu_{27.5}$ metallic glass at both the Zr and Cu K-edges has been reported [145] and insight has been obtained on the changes of the short-range order prior to crystallization.

5.4. Group IV liquids and III–V compounds

At ambient conditions group IV elements such as Si and Ge and III–V compounds are semiconductors with diamond (zinc-blende) structure. Upon melting they transform into metallic liquids with a coordination of about 6–7 intermediate between four and that of close packed metals. In these melts covalent and metallic bonding coexists as indicated by modern *ab initio* MD simulations [125]. Following pioneering studies on liquid Ge [70] a complete investigation of the structure of (solid and) liquid Ge in the temperature range 950–1600 K (including the undercooled liquid state) was made using Ge/BN powder mixtures [71]. As fully illustrated in section 4.4, by using the data analysis method previously described [123] it was possible to obtain short-range $g(r)$ functions [71] in excellent agreement with previous neutron diffraction data [124] and computer simulations [125]. Owing to the wide temperature range of the experiment [71] it was possible to reveal noticeable changes in the signal intensity, associated with the sharpening of the first-neighbour peak by lowering the temperature. The occurrence of undercooling of the Ge samples up to 250–300 K below T_m has been further demonstrated using x-ray absorption temperature scans [73,74]. An even deeper undercooling has recently been achieved by fast quenching and acquisition through a dispersive EXAFS setup [146].

GaSb and InSb are among the few III–V compounds that can be studied in vacuum and they were investigated using powder mixtures of the compounds with LiF (chemical reactions occur in other matrices such as BN or graphite) by a Chinese group [147]. Due to structural complexity the spectra were analysed by the RMC method, and detailed information could be retrieved. Atoms are found to be essentially heterocoordinated with an average coordination number between five and six. The first shell of $g_{GaSb}(r)$ is peaked around 2.7 Å and has a shoulder at 3.2 Å. In a successive paper [130], atomic configurations from RMC were used to calculate the near-edge structure spectra. These calculations, found to be in agreement with experimental data, allow for the assignment of the edge spectral features and provide further insight into the electronic density of states of the RMC model that fits the EXAFS data. A similar investigation has been performed on the near-edge structure spectra of liquid Ge [148].

5.5. Chalcogens and their alloys

Most of our present understanding of the physics of Se, Te and their alloys is due to the valuable efforts of Japanese groups that have been investigating these systems for many years. Pure Se and Te are twofold coordinated semiconductors and the tendency to form chains (helical chains in the solids) persists in the melts. The first EXAFS study of liquid Se, Te and their alloys was performed at ambient pressure [149]. The EXAFS spectra were analysed in terms of Gaussian shells. A single shell was found to be sufficient for Se, whereas a two-shell model accounting for short and long Te–Te bonds was introduced for Te [149].

Liquid Te has been the subject of successive investigations [72] in the form of 0.01 μm particles isolated in an alkali halide matrix, able to be undercooled by about 200 K below T_m. Still the double Gaussian shell data analysis model was adopted for the data interpretation. The physical difference between short and long bonds and the apparent increase of the former component upon undercooling has been interpreted as a key element driving the metal–semiconductor transition in the undercooled liquid range. The experimental data were more recently re-analysed [150] using the cumulant expansion method re-obtaining strong evidence for the short- and long-bond populations. In an independent experiment on solid and liquid Te [151] we have shown the possibility of performing an alternative data analysis [123] able to retrieve a realistic $g(r)$ function for liquid Te. The short-range part of such an improved distribution function is in fair agreement with previous EXAFS determinations [72, 149]; the region above the first-neighbour peak is certainly better described in [151] due to the presence of a realistic tail. The existence of two-bond populations in this system is quite reasonable, but strictly speaking (similarly to the Ge case illustrated in section 4.4), it is not possible to attribute a physical meaning to a multi-shell data analysis model if the resulting peaks are overlapping.

Very interesting investigations have also been performed on fluid Se close to the critical point through the semiconductor–metal–insulator sequence of transitions using the high-pressure autoclave method [51]. In a first experiment on high-density Se vapour [152] Se_2 dimers were clearly identified. Measurements performed at $P = 60$ MPa as a function of temperature along a supra-critical isobar through the semiconductor to metal transition [153] have shown that the twofold coordinated structure of the normal liquid is largely preserved, but a bond shortening by about 0.1 Å is observed in the transition region. Data analysis was here performed with the cumulant expansion approach and this is probably the reason for a strange result (with a negative asymmetry) reported for the Se–Se distribution function at 1400 °C (figure 10 of [153]). Recent tight-binding molecular dynamics simulations [154] were found to generate EXAFS signals in agreement with the experimental data but with realistic $g(r)$.

Se and Te have also been studied up to 8 GPa by another Japanese group using a cubic-type multi-anvil apparatus (MAX90) [155–157]. At high pressure the inter-chain distance in Se shortens and the liquid is found to resemble liquid Te at ambient pressures.

Te alloys such as Se–Te [158], In–Te [159] and very recently As–Te [160] have been studied extensively to reveal structural transformations as a function of temperature and composition. In particular the As–Te system has been studied combining electrical and EXAFS measurements to elucidate the nature of a semiconductor to metal transition.

5.6. Molten salts

The development of the isotopic substitution technique for neutron diffraction (ND) has historically offered a unique structural probe able to separate the partial $g_{\alpha\beta}(r)$ for a molten salt thus providing a deep insight into the physics of these systems [115]. EXAFS spectroscopy

on the other hand can provide valuable complementary information that can be very useful, especially in those cases where the contrast between different isotopically substituted samples is not sufficient for the accurate separation of the partials.

Early EXAFS applications to molten superionic compounds such as CuCl [161] have indicated the presence of a narrow Cu–Cl first-neighbour distribution with respect to the alkali halide case.

Molten $ZnCl_2$, RbCl and Rb_2ZnCl_4 were investigated by EXAFS with the aim of understanding whether the local structure of the latter is retained upon melting or whether it is better described by a mixture of the molten structures of the former binary compounds [162]. The analysis was performed using a peak fitting approach with some difficulties at the Rb K-edge for the double-electron excitation contribution. However the existence of $ZnCl_4$ units was established and differences between the spectra of the two Zn compounds suggested the absence of a tetrahedral network in molten Rb_2ZnCl_4. Another group has performed various experiments on alkali halides [163] and on KBr in particular [120], where the EXAFS signals were compared with molecular dynamics simulations based on classical potentials for various temperatures.

In a more recent investigation on CuBr [164, 165] the EXAFS spectra collected at both the Cu and Br K-edges were analysed simultaneously providing evidence for a Cu–Br first-neighbour peak much narrower than previously reported on the basis of a maximum entropy analysis of ND data. The EXAFS result is still compatible with the ND data, but, due to the greater short-range sensitivity these structural features are better observed in EXAFS than in the partial structure factors obtained from a maximum entropy analysis of the ND data. Subsequent investigations on this melt have confirmed the correctness of the EXAFS result. This case is a good example which illustrates the power of EXAFS, provided a proper data analysis is performed, and its complementarity with respect to ND. A similar investigation on the AgBr compound was recently published [166] where a careful simultaneous analysis at both the Ag and Br K-edges was performed leading to a considerable improvement with respect to previous EXAFS investigations both for the solid and molten phases.

5.7. Solutions and supercritical water

The study of aqueous solutions has been a classical field of investigation for x-ray and neutron diffraction techniques. Due to the simplicity of the experimental setup EXAFS has been also widely applied to investigate the local environment around solute species and a complete review of these applications in addition to the references already cited would go beyond the scope of this paper. Of particular methodological relevance are the investigations carried out by D'Angelo and co-workers mostly employing comparisons with molecular dynamics simulations, structural refinements and accounts of double-electron excitations [88, 89, 116, 133, 134].

The solvation of ions and molecules in supercritical water has attracted considerable interest from both the fundamental chemical and physical points of view and also from the geochemical relevance of reproducing hydrothermal conditions in the laboratory. A systematic investigation of the hydration structure around several ions has been performed by a North American group on Sr^{2+} [46], Rb^+ [167], Br^- [168] and Ni^{2+} [169]. The data analysis methods adopted by this group have progressively improved from Gaussian single-shell fits to cumulant expansion approaches to comparisons between experiment and molecular dynamics simulations. The coordination numbers reported for the Br–O coordination [168] decrease considerably towards supercritical conditions. In a very recent investigation on Br^- [170] experimental data in agreement with the previous investigation have been obtained, but in

contrast with the previous work [168] the analysis, performed through a comparison with MD simulations, reveals the persistence of a strong hydration at supercritical conditions [170]. It is clear that also in these cases the first hydration shell is not isolated and account has to be taken for the continuous distribution of neighbours, as extensively discussed in this review.

Other investigations on Ag$^+$ ions [45] and SrCl$_2$ [171] in hydrothermal conditions have been also reported.

5.8. Hydrophobic hydration

Apolar solutes such as noble gases present an anomalous solubility behaviour in water with a solubility minimum around 80–100 °C. Thermodynamical considerations indicate the presence of large negative entropic contributions to the free energy associated with the hydrophobic solvation of the noble gas atom, especially at low temperature. In other words it is believed that the introduction of the gas atoms increases the order in the water network. Due to the small solubilities these ideas have for a long time eluded any experimental verification. XAS is clearly the ideal probe for such a dilute solubility case and excellent contrast can be achieved at the Kr and Xe K-edges. The first attempt to measure Kr in H$_2$O was made on supercritical water [46] without observing any structural signal (experiment possibly to be repeated). More recent experiments were performed by pressurizing Kr on water at room temperature (up to about 10 MPa) and a clear signal from the Kr–O partial $g(r)$ was detected allowing the short-range shape of this function to be determined for the first time from experiment [43]. In a successive temperature-dependent experiment made up to about 80 °C at both the Kr and Xe K-edges [172] a dramatic temperature dependence of the EXAFS has been observed that implies a strong disordering of the hydration shell in this temperature range, thus providing the first microscopic structural basis for the understanding of the solubility data. In a subsequent investigation with the combined action of pressure and temperature it has been possible to form a clathrate ice structure [173] and compare the Kr environment in the solid phase with that in the liquid.

5.9. Molecular fluids

In spite of the early historical application of EXAFS to molecular liquids [10] this promising research field is still largely unexploited. In most cases the dominance of intra-molecular correlations with respect to inter-molecular contacts limits the EXAFS sensitivity to the molecular structure and makes the spectra of molecular liquids very similar to those of the corresponding vapours. Still, however, the exceptional sensitivity of EXAFS to molecular structures, down to the 0.001 Å range for first neighbours [109], allows one to detect even very small changes in the molecular structures among different phases. EXAFS actually possess the unique characteristic of being applicable indifferently to gaseous, liquid and solid specimens, and in all of these cases with the same structural sensitivity. By comparison gas-phase electron diffraction and x-ray/neutron diffraction methods for liquids and solids are sensitive in a quite different manner to molecular bond-lengths.

Homonuclear diatomic molecules have been widely studied by EXAFS and clear bond length differences have been detected in the case of Br$_2$ [48] and more recently I$_2$ [174], both among different phases and in the liquid phase as a function of the density. Iodine is actually a very interesting molecular fluid due to a strong tendency for charge-transfer which makes the I–I bond length distribution a sensitive probe of inter-molecular interactions. This sensitivity has been exploited in an investigation of fluid I$_2$ along the liquid–vapour coexistence curve [52] and successively in a high-P and high-T study towards the fluid metallization

transition region [175]. The relevance of the density parameter in explaining the measured bond length data has been emphasized [176].

6. Perspective and open problems

The overall scenario of the research on the liquid state of matter by using EXAFS spectroscopy reviewed in this article suggests the existence of a very fertile and expanding research field. However, a fair review should not hide a certain number of open problems that will have to be tackled in the next few years.

(a) There is great confusion in the EXAFS community regarding the meaning of a radial distribution function (often confused with the magnitude of the Fourier transform) and how data on a disordered system (such as a liquid or a glass) can be analysed in terms of a $g(r)$. The object of this review was, in part, to clarify this point. There is no scope for analysing liquid phase spectra by extracting parameters of isolated shells since no meaningful comparison can be made with a $g(r)$. Also peak modelling on top of a $g(r) = 0$ baseline is not adequate, because it tends to underestimate coordination numbers. We have shown how the simplicity of the peak fitting approach can be recovered provided that the peaks are modelled on top of a $g(r) = g_{tail}(r) \neq 0$ baseline which, together with a set of constraints on the parameters, guarantees the correct long-range behaviour of an atomic distribution. This approach has been successfully adopted in numerous papers but is still ignored by a large part of the community that continues to provide structural results for liquids in terms of the parameters (or cumulants) of isolated peaks which often result in unphysical distributions. Of course this is just a first step and there is a wide open research field for the development of more sophisticated data analysis procedures able to exploit the short-range structural sensitivity of EXAFS to provide realistic model atomic distributions (also by combining several experimental inputs) and direct information on the inter-atomic potentials.

(b) The major limitation of the present theory is its inability to predict the accurate shape of the atomic background underlying the structural signal. This problem has been systematically hidden or neglected in a large part of the published research. The errors resulting from this practice will have to be checked for an assessment of the validity of many published results. The empirical methods proposed for the background subtraction are, on the other hand, very effective, but a more rigorous basis for these procedures and additional investigations are desirable. As a minimal requirement however, the authors should publish clear diagrams showing the atomic background adopted to isolate the $\chi(k)$ signal, otherwise detailed comparisons will hardly be possible at later times.

In some way we have to admit that most of the present difficulties in the full understanding and exploitation of EXAFS come from the complexity of the phenomenon, which, even if dominated by interference effects resulting from photoelectron scattering, is altered by other effects whose interpretation and account can only be made at present on an empirical basis. It is quite singular, but in a sense true, to state that in the year 2000 some of our troubles are not so different from those which puzzled our predecessors around the year 1930. On the other hand, enormous advances in the spectroscopy have occurred as summarized by the following three main achievements.

(1) On the experimental side, reliable techniques have been developed for the most diverse applications which extend the possible range of measurable specimens to basically all liquid substances including reactive species and covering a wide range of pressures and

temperatures. These achievements have benefited from the availability of third generation synchrotron radiation sources where advanced experimental stations integrating several experimental techniques, required for *in situ* sample characterization, have been built. It is expected that, in the near future, all these techniques will be further improved and widely exploited providing a large number of new reliable experimental data on liquid systems which can hardly be investigated by other means.

(2) From the theoretical side, the availability of a reliable theoretical framework for the data interpretation allows for the use of this spectroscopy to derive valuable short-range structural information. The success of the theory to reproduce the spectra of simple molecular or crystalline systems is a proof of the validity of the theory and of the underlying approximations. The same theory can therefore be used to derive information on atomic distributions in liquids (and glasses). In the scenario of the various data analysis procedures proposed for application to the liquid phase, some of them are emerging as able to provide reliable information directly comparable with theoretically predicted (or simulated) radial distributions.

(3) Out of the numerous applications of EXAFS to liquids several of them have already provided novel information and/or improved previous structural knowledge from diffraction experiments. Some experiments gave the first experimental information on systems that, because of the low concentration or other experimental difficulties, could not be investigated by other means. Complementarity between EXAFS and x-ray or neutron diffraction techniques has been clearly demonstrated in several cases including multi-component systems.

As a conclusion to this review, it is not unfair to state that our present physical knowledge and understanding of the liquid state of matter can greatly benefit from the maturity, eventually reached after nearly a century, of this fascinating spectroscopic technique.

Acknowledgments

References

[1] Fricke H 1920 *Phys. Rev.* **16** 202
[2] Kronig R de L 1931 *Z. Phys.* **70** 317
[3] Kronig R de L 1932 *Z. Phys.* **75** 191
[4] Kronig R de L 1932 *Z. Phys.* **75** 468
[5] Hartree D R, Kronig R de L and Petersen H 1934 *Physica* **1** 895
[6] Stumm von Bordwehr R 1989 *Ann. Phys., Paris* **14** 377
[7] Yost D M 1929 *Phil. Mag.* **8** 845
[8] Hanawalt J D 1931 *Phys. Rev.* **37** 715
[9] Cioffari B 1937 *Phys. Rev.* **51** 630
[10] Dryński T and Smoluchowski R 1939 *Physica* **6** 929
[11] Dryński T and Smoluchowski R 1940 *Phys. Rev.* **58** 207
[12] Sawada M, Tsutsumi K, Shiraiwa T and Obashi M 1955 *J. Phys. Soc. Japan* **10** 464
[13] Shiraiwa T, Ishimura T and Sawada M 1957 *J. Phys. Soc. Japan* **12** 788
[14] Nelson W F, Siegel I and Wagner R W 1962 *Phys. Rev.* **127** 2025

[15] Brümmer O and Dräger G 1968 *Phys. Status Solidi* **27** 513
[16] Sayers D E, Stern E A and Lytle F W 1971 *Phys. Rev. Lett.* **27** 1204
[17] Kinkaid B M and Eisenberger P 1975 *Phys. Rev. Lett.* **34** 1361
[18] Eisenberger P and Kinkaid B M 1975 *Chem. Phys. Lett.* **36** 134
[19] Sandstrom D R, Dodgen H W and Lytle F W 1977 *J. Chem. Phys.* **67** 473
[20] Sandstrom D R 1979 *J. Chem. Phys.* **71** 2381
[21] Fontaine A, Lagarde P, Raoux D, Fontana M P, Maisano G, Migliardo P and Wanderlingh F 1978 *Phys. Rev. Lett.* **41** 504
[22] Lagarde P, Fontaine A, Raoux D, Sadoc A and Migliardo P 1980 *J. Chem. Phys.* **72** 3061
[23] Petersen H and Kunz C 1975 *Phys. Rev. Lett.* **35** 863
[24] Petersen H and Kunz C 1977 *J. Phys. F: Met. Phys.* **7** 2495
[25] Crozier E D, Lytle F W, Sayers D E and Stern E A 1977 *Can. J. Chem.* **55** 1968
[26] Crozier E D and Seary A J 1980 *Can. J. Phys.* **58** 1388
[27] Boyce J B, Hayes T M, Stutius W and Mikkelsen J C Jr 1977 *Phys. Rev. Lett.* **38** 1362
[28] Hayes T M, Boyce J B and Beeby J L 1978 *J. Phys. C: Solid State Phys.* **11** 2931
[29] Hayes T M and Boyce J B 1980 *J. Phys. C: Solid State Phys.* **13** L731
[30] Hayes T M and Boyce J B 1981 *Phys. Rev. B* **23** 2876
[31] Boyce J B, Hayes T M Mikkelsen J C Jr and Stutius W 1980 *Solid State Commun.* **33** 183
[32] Raoux D, Petiau J, Bondot P, Calas G, Fontaine A, Lagarde P, Levitz P, Loupias G and Sadoc A 1980 *Revue Phys. Appl.* **15** 1079
[33] Lee P A, Citrin P H, Eisenberger P and Kincaid B M 1981 *Rev. Mod. Phys.* **53** 769
[34] Hayes T M and Boyce J B 1982 *Solid State Physics, vol 37* ed H Ehrenreich, F Seitz and D Turnbull (New York: Academic) pp 173–351
[35] Teo B K and Joy D C (eds) 1981 *EXAFS Spectroscopy* (New York: Plenum)
[36] Crozier E D, Rehr J J and Ingalls R 1988 *X-Ray Absorption: Principles, Applications Techniques of EXAFS, SEXAFS and XANES* ed D C Koningsberger and R Prins (New York: Wiley) pp 375–84
[37] Rehr J J and Albers R C 2000 *Rev. Mod. Phys.* **72** 621
[38] Stern E A and Kim K 1981 *Phys. Rev. B* **23** 3781
[39] Goulon J, Goulon Ginet C, Cortes R and Dubois M 1982 *J. Physique* **43** 539
[40] Ottaviano L, Filipponi A and Di Cicco A 1994 *Phys. Rev. B* **49** 11749
[41] Filipponi A and Di Cicco A 1994 *Nucl. Instrum. Methods Phys. Res. B* **93** 302
[42] Sánchez E Marcos, Gil M, Martínez J M, Muñoz-Páez A and Sánchez Marcos A 1994 *Rev. Sci. Instrum.* **65** 2153
[43] Filipponi A, Bowron D T, Lobban C and Finney J L 1997 *Phys. Rev. Lett.* **79** 1293
[44] Bowron D T, Weigel R, Filipponi A, Roberts M A and Finney J L 2001 *Mol. Phys.* **99**
[45] Seward T M, Henderson C M B, Charnock J M and Dobson B R 1996 *Geochim. Cosmochim. Acta* **60** 2273
[46] Pfund D M, Darab J G, Fulton J L and Ma Y 1994 *J. Phys. Chem.* **98** 13102
[47] Ertel T S and Bertagnolli H 1993 *Nucl. Instrum. Methods Phys. Res. B* **73** 199
[48] Filipponi A, Ottaviano L, Passacantando M, Picozzi P and Santucci S 1993 *Phys. Rev. E* **48** 4575
[49] Wallen S L, Pfund D M, Fulton J L and Yonker C R 1996 *Rev. Sci. Instrum.* **67** 2843
[50] Murata T, Nakagawa K, Kimura A, Otoda N and Shimoyama I 1995 *Rev. Sci. Instrum.* **66** 1437
[51] Tamura K, Inui M and Hosokawa S 1995 *Rev. Sci. Instrum.* **66** 1382
[52] Buontempo U, Filipponi A, Postorino P and Zaccari R 1998 *J. Chem. Phys.* **108** 4131
[53] Ingalls R, Garcia G A and Stern E A 1978 *Phys. Rev. Lett.* **40** 334
[54] Ingalls R, Crozier E D, Whitmore J E, Seary A J and Tranquada J M 1980 *J. Appl. Phys.* **51** 3158
[55] Werner A, Hochheimer H D and Lengeler B 1982 *Rev. Sci. Instrum.* **53** 1467
[56] Itié J P 1992 *Phase Transitions* **39** 81
[57] Dartyge E, Depautex C, Dubuisson J M, Fontaine A, Jucha A, Leboucher P and Tourillon G 1986 *Nucl. Instrum. Methods Phys. Res. A* **246** 452
[58] Tolentino H, Baudelet F, Dartyge E, Fontaine A, Lena A and Tourillon G 1990 *Nucl. Instrum. Methods Phys. Res. A* **289** 307
[59] Besson J M, Nelmes R J, Hamel G, Loveday J S, Weill G and Hull S 1992 *Physica B* **180/181** 907
[60] Katayama Y, Mezouar M, Itié J P, Besson J M, Syfosse G, Le Fevre P and Di Cicco A 1997 *J. Physique Coll. IV* **7** C2 1011
[61] Filipponi A, Borowski M, Bowron D T, Ansell S, De Panfilis S, Di Cicco A and Itiè J-P 2000 *Rev. Sci. Instr.* **71** 2422
[62] Mezouar M, Le Bihan T, Libotte H, Le Godec Y and Häusermann D 1999 *J. Synchrotron Radiat.* **6** 1115
[63] Lytle F W, Wei P S P, Gregor R B, Via G H and Sinfelt J H 1979 *J. Chem. Phys.* **70** 4849

[64] Mikkelsen J C Jr, Boyce J B and Allen R 1980 *Rev. Sci. Instrum.* **51** 388
[65] Clausen B S, Steffensen G, Fabius B, Villadsen J, Feidenhans'l R and Topsœ H 1991 *J. Catal.* **132** 524
[66] Moggridge G D, Schroeder S L M and Lambert R M 1995 *Nucl. Instrum. Methods Phys. Res.* B **97** 28
[67] Di Cicco A, Aquilanti G, Minicucci M, Filipponi A and Rybicki J 1999 *J. Phys.: Condens. Matter* **11** L43
[68] Farges F, Itiè J-P, Fiquet G and Andrault D 1995 *Nucl. Instrum. Methods Phys. Res.* B **101** 493
[69] F Farges, Brown G E Jr, Navrotsky A, Gan H and Rehr J R 1996 *Geochim. Cosmochim. Acta* **60** 3055
[70] Orton B R 1990 *Neutron and X-Ray Scattering: Complementary Techniques (Inst. Phys. Conf. Ser. 101)* (Bristol: Institute of Physics) p 77
[71] Filipponi A and Di Cicco A 1995 *Phys. Rev. B* **51** 12322
[72] Tsuzuki T, Yao M and Endo H 1995 *J. Phys. Soc. Japan* **64** 485
[73] Filipponi A 1996 *J. Phys.: Condens. Matter* **8** 9335
[74] Filipponi A, Borowski M, Loeffen P W, De Panfilis S, Di Cicco A, Sperandini F and Giorgetti M 1998 *J. Phys.: Condens. Matter* **10** 235
[75] De Panfilis S and Filipponi A 2000 *J. Appl. Phys.* **88** 562
[76] Itiè J P 1999 *Technologie des Hautes Pressions, CNRS* ed J C Cervin, R Argoud and S Le Floch (Paris: Launay) pp 55–75
[77] Herlach D M 1991 *Annu. Rev. Mater. Sci.* **21** 23
[78] Jacobs G, Egry I, Maier K, Platzek D, Reske J and Frahm R 1996 *Rev. Sci. Instrum.* **67** 3683
[79] Krishnan S and Price D L 1997 *J. Phys.: Condens. Matter* **12** R145
[80] Landron C, Launay X, Rifflet J C, Echegut P, Auger Y, Ruffier D, Coutures J P, Lemonier M, Gailhanou M, Bessiere M, Bazin D and Dexpert H 1997 *Nucl. Instrum. Methods Phys. Res.* B **124** 627
[81] Bagus P S 1965 *Phys. Rev. A* **139** 619
[82] Åberg T 1967 *Phys. Rev.* **156** 35
[83] Ito Y, Mukoyama T, Emura S, Takahashi M, Yoshikado S and Omote K 1995 *Phys. Rev. A* **51** 303
[84] Giglio E, Loreti S and Pavel N V 1988 *J. Phys. Chem.* **92** 2858
[85] Tanida H, Sakane H, Watanabe I and Yokoyama Y 1993 *Chem. Lett.* **10** 1647
[86] Solera J A, García J and Proietti M G 1995 *Phys. Rev. B* **51** 2678
[87] Filipponi A and Di Cicco A 1995 *Phys. Rev. A* **52** 1072
[88] D'Angelo P, Nolting H and Pavel N V 1996 *Phys. Rev. A* **53** 798
[89] D'Angelo P, Pavel N V, Roccatano D and Nolting H 1996 *Phys. Rev. A* **54** 12129
[90] Rehr J J, Stern E A, Martin R L and Davidson E R 1978 *Phys. Rev. B* **17** 560
[91] Chou S, Rehr J J, Stern E A and Davidson E R 1987 *Phys. Rev. B* **35** 2604
[92] Lu D and Rehr J J 1988 *Phys. Rev. B* **37** 6126
[93] Tyson T A, Hodgson K O, Natoli C R and Benfatto M 1992 *Phys. Rev. B* **46** 5997
[94] Hedin L and Lundqvist B I 1971 *J. Phys. C: Solid State Phys.* **4** 2064
[95] Hayes T M, Sen P N and Hunter S H 1976 *J. Phys. C: Solid State Phys.* **9** 4357
[96] Schaich W L 1973 *Phys Rev. B* **8** 4028
[97] Lee P A and Pendry J B 1975 *Phys. Rev. B* **11** 2795
[98] Natoli C R and Benfatto M 1986 *J. Physique Coll.* **47** C8 11
[99] Fonda L 1992 *J. Phys.: Condens. Matter* **4** 8269
[100] Faulkner J S and Stocks G M 1980 *Phys. Rev. B* **21** 3222
[101] Benfatto M, Natoli C R, Bianconi A, Garcia J, Marcelli A, Fanfoni M and Davoli I 1986 *Phys. Rev.* B **34** 5774
[102] Brouder C, Ruiz-López M F, Pettifer R F, Benfatto M and Natoli C R 1989 *Phys. Rev. B* **39** 1488
[103] Citrin P H, Eisenberger P and Kincaid B M 1976 *Phys. Rev. Lett.* **36** 1346
[104] Filipponi A, Di Cicco A and Natoli C R 1995 *Phys. Rev. B* **52** 15122
[105] Schaich W L 1984 *Phys. Rev. B* **29** 6513
[106] Gurman S J, Binsted N and Ross I 1984 *J. Phys. C: Solid State Phys.* **17** 143
[107] Filipponi A and Di Cicco A 1995 *Phys. Rev. B* **52** 15135
[108] Benfatto M, Natoli C R and Filipponi A 1989 *Phys. Rev. B* **40** 9626
[109] Filipponi A and D'Angelo P 1998 *J. Chem. Phys.* **109** 5356
[110] Natoli C R, Benfatto M and Doniach S 1986 *Phys. Rev. A* **34** 4682
[111] Foulis D L, Pettifer R F, Natoli C R and Benfatto M 1990 *Phys. Rev. A* **41** 4682
[112] Foulis D L, Pettifer R F and Sherwood P 1995 *Europhys. Lett.* **29** 647
[113] Joly Y, Cabaret D, Renevier H and Natoli C R 1999 *Phys. Rev. Lett.* **82** 2398
[114] Filipponi A 1995 *Physica* B **208/209** 29
[115] Enderby J E 1983 *Contemp. Phys.* **24** 561
[116] D'Angelo P, Di Nola A, Filipponi A, Pavel N V and Roccatano D 1994 *J. Chem. Phys.* **100** 985
[117] Palmer B J, Pfund D M and Fulton J L 1996 *J. Phys. Chem.* **100** 13393

[118] Eisenberger P and Brown G S 1979 *Solid State Commun.* **29** 481
[119] Yang D S, Fazzini D R, Morrison T I, Tröger L and Bunker G 1997 *J. Non-Cryst. Solids* **210** 275
[120] Di Cicco A, Rosolen M J, Marassi R, Tossici R, Filipponi A and Rybicki J 1996 *J. Phys.: Condens. Matter* **8** 10779
[121] Bunker G 1983 *Nucl. Instrum. Methods* **207** 437
[122] Dalba G, Fornasini P and Rocca F 1993 *Phys. Rev.* B **47** 8502
[123] Filipponi A 1994 *J. Phys.: Condens. Matter* **6** 8415
[124] Salmon P S 1988 *J. Phys. F: Met. Phys.* **18** 2345
[125] Kresse G and Hafner J 1994 *Phys. Rev.* B **49** 14251
[126] Babanov Y A, Vasin V V, Ageev A L and Ershov N V 1981 *Phys. Status Solidi* **105** 747
[127] Babanov Y A and Shvetsov V R 1986 *J. Physique Coll.* **47** C8 37
[128] McGreevy R L and Pusztai L 1988 *Mol. Simul.* **1** 359
[129] Gurman S J and McGreevy R L 1990 *J. Phys.: Condens. Matter* **2** 9463
[130] Li C, Lu K and Wang Y 1999 *J. Phys.: Condens. Matter* **11** 3013
[131] Barocchi F, Chieux P, Magli R, Reatto L and Tau M 1993 *Phys. Rev. Lett.* **70** 947
[132] Yokoyama T 1998 *Phys. Rev.* B **57** 3423
[133] Filipponi A, D'Angelo P, Pavel N V and Di Cicco A 1994 *Chem. Phys. Lett.* **225** 150
[134] D'Angelo P and Pavel N V 1999 *J. Chem. Phys.* **111** 5107
[135] Di Cicco A and Filipponi A 1994 *Europhys. Lett.* **27** 407
[136] Greaves G N, S J.Gurman, Catlow C R A, Chadwick A V, Houde-Walter S, Henderson C M B and Dobson B R 1991 *Philos. Mag. A* **64** 1059
[137] Mobilio S and Meneghini C 1998 *J. Non-Cryst. Solids* **232–234** 25
[138] Di Cicco A, Filipponi A, Itiè J P and Polian A 1996 *Phys. Rev.* B **54** 9086
[139] Orton B R, Malra G K and Steel A T 1987 *J. Phys. F: Met. Phys.* **17** L45
[140] Stern E A, Līviņš P and Zhang Z 1991 *Phys. Rev.* B **43** 8850
[141] Di Cicco A 1996 *Phys. Rev.* B **53** 6174
[142] Filipponi A, Di Cicco A and De Panfilis S 1999 *Phys. Rev. Lett.* **83** 560
[143] Filipponi A, De Panfilis S and Di Cicco A 2000 *Phys. Status Solidi* b **219** 267
[144] Jacobs G and Egry I 1999 *Phys. Rev.* B **59** 3961
[145] Schumacher H, Herr U, Oelgeschlaeger D, Traverse A and Samwer K 1997 *J. Appl. Phys.* **82** 155
[146] Pascarelli S, De Panfilis S and Neisius T 2000 *Phys. Rev.* B **62** 3717
[147] Wang Y, Lu K and Li C 1997 *Phys. Rev. Lett.* **79** 3664
[148] Li C, Lu K, Wang Y, Tamura K, Hosokawa S and Inui M 1999 *Phys. Rev.* B **59** 1571
[149] Tamura K, Inui M, Yao M, Endo H, Hosokawa S, Hoshino H, Katayama Y and Maruyama K 1991 *J. Phys.: Condens. Matter* **3** 7495
[150] Kawakita Y, Yao M and Endo H 1999 *J. Non-Cryst. Solids* **250–252** 447
[151] De Panfilis S and Filipponi A 1997 *Europhys. Lett.* **37** 397
[152] Hosokawa S, Tamura K, Inui M, Yao M, Endo H and Hoshino H 1992 *J. Chem. Phys.* **97** 786
[153] Soldo Y, Hazemann J L, Aberdam D, Inui M, Tamura K, Raoux D, Pernot E, Jal J F and Dupuy-Philon J 1998 *Phys. Rev.* B **57** 258
[154] Raty J Y, Saul A, Gaspard J P and Bichara C 1999 *Phys. Rev.* B **60** 2441
[155] Katayama Y, Tsuji K, Oyanagi H and Shimomura O 1998 *J. Non-Cryst. Solids* **232–234** 93
[156] Tsuji K and Katayama Y 1998 *The Physics of Complex Liquids* ed F Yonezawa, K Tsuji, K Kaji, M Doi and T Fujiwara (New York: World Scientific) pp 83–97
[157] Katayama Y, Shimomura O and Tsuji K 1999 *J. Non-Cryst. Solids* **250–252** 537
[158] Endo H, Tamura K and Yao M 1987 *Can. J. Phys.* **65** 266
[159] Kawakita Y, Matsubara R, Nakashima H and Takeda S 1998 *J. Non-Cryst. Solids* **232–234** 483
[160] Endo H, Hoshino H, Ikemoto H and Miyanaga T 2000 *J. Phys.: Condens. Matter* **12** 6077
[161] Boyce J B and Mikkelsen J C Jr 1984 *Physics and Chemistry of Electrons and Ions in Condensed Matter, Proc. NATO Advanced Study Inst.* ed J V Acrivos, N F Mott and A D Yoffe (Dordrecht: Reidel) pp 273–7
[162] Li H, Lu K, Wu Z and Dong J 1994 *J. Phys.: Condens. Matter* **6** 3629
[163] Di Cicco A, Berrettoni M, Marassi R, Tossici R and Filipponi A 1994 *Proc. 9th Int. Symp. on Molten Salts* vol 94-13, ed C L Hussey, D S Newman, G Mamantov and Y Ito (Pennington, NJ: Electrochemical Society) p 77
[164] Di Cicco A, Minicucci M and Filipponi A 1997 *Phys. Rev. Lett.* **78** 460
[165] Di Cicco A and Minicucci M 1997 *Phys. Rev.* B **56** 11456
[166] Di Cicco A, Taglienti M, Minicucci M and Filipponi A 2000 *Phys. Rev.* B **62** 12001
[167] Fulton J L, Pfund D M, Wallen S L, Newville M, Stern E A and Ma Y 1996 *J. Chem. Phys.* **105** 2161

[168] Wallen S L, Palmer B J, Pfund D M, Fulton J L, Newville M, Ma Y and Stern E A 1997 *J. Phys. Chem.* A **101** 9632

[169] Wallen S L, Palmer B J and Fulton J L, 1998 *J. Chem. Phys.* **108** 4039

[170] Ferlat G, San Miguel A, Jal J F, Soetens J C, Bopp P A, Daniel I, Guillot S, Hazemann J L and Argoud R 2001 *Phys. Rev.* B **63**

[171] Seward T M, Henderson C M B, Charnock J M and Driesner T 1999 *Geochim. Cosmochim. Acta* **63** 2409

[172] Bowron D T, Filipponi A, Lobban C and Finney J L 1998 *Chem. Phys. Lett.* **293** 33

[173] Bowron D T, Filipponi A, Roberts M A and Finney J L 1998 *Phys. Rev. Lett.* **81** 4164

[174] Buontempo U, Di Cicco A, Filipponi A, Nardone M and Postorino P 1997 *J. Chem. Phys.* **107** 5720

[175] Buontempo U, Filipponi A, Martínez-García D, Postorino P, Mezouar M and Itiè J P 1998 *Phys. Rev. Lett.* **80** 1912

[176] Postorino P, Buontempo U, Filipponi A and Nardone M 1999 *Physica* B **265** 72